Journal of Energy Storage 39 (2021) 102645

Contents lists available at ScienceDirect

Journal of Energy Storage

journal homepage: www.elsevier.com/locate/est

Multicomponent bio-based fatty acids system as phase change material for low temperature energy storage

Meysam Nazari, Mohamed Jebrane *, Nasko Terziev

Department of Forest Biomaterials and Technology, Swedish University of Agricultural Sciences, Vallvägen 9C, 750 07 Uppsala, Sweden

ARTICLE INFO

Keywords:
Bio-based PCMs
Coconut oil fatty acids
Energy storage in buildings
Multicomponent mixtures

ABSTRACT

In this study, new multicomponent mixtures of fatty acids for low temperature thermal energy storage applications have been developed. The new mixtures were based on coconut oil fatty acids (CoFA) and commercial grades of oleic (OA) and linoleic acid (LA). Refined coconut oil (CO) was first converted into free fatty acids by alkaline saponification. The prepared CoFA were then mixed with OA or LA at various compositions to prepare stable bio-based phase change materials (BPCMs). The thermal behavior including melting/solidification temperatures, specific heat and enthalpy of the developed mixtures were investigated by means of differential scanning calorimetry (DSC) and T-history. Transient hot wire method was used to measure thermal conductivity of the PCMs. The chemical stability and thermal reliability of the mixtures were assessed stepwise from 100 to 700 melt/freeze cycles by attenuated total reflectance-Fourier transform infrared spectroscopy (ATR-FTIR) and DSC. Based on DSC and T-history results, the phase transition of the developed PCMs were in line with the range of human comfort temperatures i.e. 18-25 °C, with no incongruent melting and less than 0.6 °C super cooling, whereas specific heat and enthalpy of the new mixtures were in the range of 1-5 J/g K, and 40-100 J/g. The FTIR and DSC results indicated that the PCMs mixtures are chemically and thermally stable. The thermal conductivity of the mixtures were in average 0.2 W/m K, in liquid phase and 0.35 W/m K, in solid phase. Out of the different developed combinations, the mixture of LA/CoFA (20/80) showed distinguished performance and can be considered as potential BPCM for low temperature thermal energy storage applications.

1. Introduction

Increasing world populations and technologies development lead to increase in demand for energy. Moreover, environmental concerns regarding climate change have increased over the last decades. In order to address the growth in energy demands and considering environmental concerns, methods to store and manage energy are as important as searching for new energy resources [1]. Among the sectors that consume considerable energy, residential building uses over 40% of the total globally generated energy, contributing to 30% of the emitted greenhouse gases [2-4]. Managing energy consumption in building sector by maintaining the indoor temperature constant and minimizing the temperature fluctuations inside the buildings are considered as a potential solution to govern the energy consumption [5,6]. In this context, energy storage in form of latent heat thermal energy using phase change materials (PCMs) is an attractive solution due to high-energy storage density with small difference between storing and releasing functions. Several categories of materials have been investigated as PCMs, including organic compounds (fatty acids, PEG and Paraffins) and inorganic systems (salt and salt hydrates) [6-10]. These materials are widely used in building sector to control the indoor temperature fluctuations by integrating them into buildings elements [1, 6,11,12]. Most of these strategies involving incorporation of organic phase change materials (OPCMs) into construction materials mainly focused on storing and releasing solar energy for indoors heating. This pattern is suitable for regions where there is enough sun during winter periods when the demands for energy is high. However, in cold-weather countries such as Canada and Nordic countries, the sunny days during the winter periods are limited. Thus, using PCMs to control indoor temperature fluctuations in residential buildings seems more interesting than storing solar energy during daytimes and releasing it during nights in these countries.

Among the investigated OPCMs, fatty acids are considered as the most promising materials because they are renewable, non-toxic, commercially available at low cost, and biodegradable [13,14]. Furthermore, fatty acids benefit from the unique and superior characteristics such as congruent melting, chemical and thermal stability

* Corresponding author.
E-mail address: mohamed.jebrane@slu.se (M. Jebrane).

https://doi.org/10.1016/j.est.2021.102645
Received 30 November 2020; Received in revised form 23 April 2021; Accepted 27 April 2021
Available online 13 May 2021

Nomenclature

A	Contact surface area [m^2]
Bi	Biot number
c_p	Specific heat [J/g K]
D	Diameter [m]
H	Enthalpy [J/g]
h	Heat transfer coefficient [W/m^2 K]
I	Electrical current [A]
λ	Thermal conductivity [W/m K]
L	Length of the wire [m]
$LMTD$	Logarithmic mean temperature difference [K]
m	Mass of the materials [kg]
n	Time point [s]
P	Independent variables
Q	Heat [W]
R	Dependent variables
r	Radius [m]
T	Temperature [K]
t	Time [s]
U	Uncertainty
u	Overall heat transfer coefficient [W/m^2 K]
V	Voltage [V]

Greek symbol

δ	Characteristics length [m]
Δ	Difference
∞	Ambient

Subscripts

f	Final
in	Inner side
ins	Insulation
o	Initial
out	Outer side
pcm	Sample
r	Reference
tube	Tube container
tot	Total
∞	Ambient

Abbreviatio

BPCM	Bio-based phase change materials
CO	Coconut oil
CoFA	Coconut oil fatty acid
DSC	Differential scanning calorimetry
FTIR	Fourier-transform infrared spectroscopy
LA	Linoleic acid
OA	Oleic acid
OPCM	Organic phase change materials
PCM	Phase change materials

[15-17] and, thus constitute potential Bio-based PCMs (BPCMs) for low to medium temperature energy storage applications [13,14]. According to the American Society of Heating, Cooling and Air-conditioning Engineers (ASHRAE), the room temperature for summer and winter conditions are suggested to be in the range of 23.5-25.5°C and 21.0-23.0°C respectively [7]. However, most of the pure fatty acids have phase transition temperatures outside the standard temperature range [13,14], and thus cannot be used directly. By mixing two or several fatty acid together, stable mixtures with phase transition temperatures suitable for low thermal energy storage applications can be obtained. Several studies have been conducted on fatty acid mixtures to find stable mixtures as BPCMs [18-25]. Recently, capric and lauric acids were studied when incorporated into wallboards for low temperature thermal energy storage for heating and cooling applications [21]. The thermal stability of the eutectic mixture was stable after 360 cycles and can serve for latent heat storage in building applications. Another study reported that the addition of alkanes (e.g. pentadecane) to capric-lauric mixtures could enhance the thermal reliability and storage potential for cooling applications [22]. Ma et al. [20] studied the eutectic mixture of capric-palmitic acids impregnated into delignified wood and reported a retention of 61.2% without leakage, and the composite displayed a phase transition temperature of 23.4 °C and latent heat of 94.4 J/g with good thermal stability. Mathis et al. [18] investigated the performance of capric-lauric mixtures and two other commercial BPCMs packed in plastic pouches integrated into fiberboards panels. The studied BPCMs were thermally stable after thermal cycling and showed a phase transition temperature and latent heat storage appropriate for building applications. Karaipekli and Sari [23] studied mixtures of fatty acids including compositions of capric, lauric, palmitic and stearic acids, incorporated in expanded vermiculite for working temperatures in the range of 18-25 °C. The mixtures were thermally and chemically stable after 5000 cycles with melting temperatures in the range of 19.09-25.64 °C and latent heats ranging from 61.03 to 72.02 J/g, i.e. suitable for building. Similar mixtures comprising capric, lauric, myristic, palmitic and stearic acids were investigated by Sharma et al. [24]; and melting temperatures in the range 20-30°C and latent heat ranging from 100 to 160 J/g were recorded. Ke et al. [25] reported similar results for the above-mentioned binary fatty acid mixtures incorporated in polyethylene terephthalate (PET), while when tertiary compositions were prepared, different behaviors were observed [26]. Most of these combinations are promising but they suffer from phase separation in solid phase due to the immiscibility of the two fatty acid species [27,28].

Some tropical fruit oils and their derivatives have been recently investigated as a promising bio resourced PCMs. In this context, several studies reported the potential of palm kernel oil, Allanblackia, shea butter and coconut oil as promising phase change materials for building applications [29-32]. Most of these plant oils are polymorphic with a multiple melting/freezing profile over the transition temperatures. Moreover, some of the studied oils are susceptible to oxidation hence limiting their application as PCMs in buildings [29]. Kahwaji and White [33] investigated the feasibility of using a series of edible oils including coconut oil as PCM. They concluded that coconut oil showed a good thermal and chemical stability after 200 melting/freezing cycles with reliable latent heat of fusion and phase transition temperature. However, the DSC results showed that coconut oil melts and freezes quit incongruently at the desired temperature range. The key limitation for coconut oil is the large supercooling in addition to the transition temperatures, which are slightly outside the temperatures of interest (i.e. 20-25 °C) that is typically required to control temperature fluctuations in buildings. Nonetheless, if converted to free fatty acids, these bio-oils can be used as PCM for low thermal energy storage in building applications.

To overcome the limitation of coconut oil as PCM to control energy intermittency inside residential buildings hence using energy more efficiently, new mixtures with a phase transition temperature in the range of human comfort temperatures were prepared. These new mixtures were based on coconut oil fatty acids, technical oleic and linoleic acids.

2. Experimental

2.1. Materials

Refined coconut oil (CO) and technical linoleic acid (LA) (60%) were purchased from Acros. Purified oleic acid (80%), sodium hydroxide, and sulfuric acid (95-98%) were purchased from VWR, Merck and sigma-Aldrich, respectively. All other solvents were ACS-grade and used without further purification. Coconut oil free fatty acids (CoFA) were prepared by a conventional alkaline saponification followed by neutralization using sulfuric acid and extracted with n-hexane.

Fatty acid mixtures were prepared by weighing and mixing of CoFA and OA or LA into a glass vial, and dissolved in a minimum amount of n-hexane. After complete dissolution of the fatty acids species, the solvent was removed by evaporation under reduced pressure. After complete removal of solvent, the mixtures were melted at 40 °C and freezed at -20 °C to avoid phase separation. This process of heating (40 °C) and cooling (-20 °C) was repeated several times to maximize homogeneity.

2.2. Methods

2.2.1. Fourier Transform Infrared spectroscopy (FTIR-ATR)

Characteristic functional groups of CO and CoFA as well as those of the commercial fatty acids and the mixtures were examined by a Spectrum one FTIR instrument (Perkin Elmer) equipped with an UATR Diamond accessory allowing collection of FTIR spectra without prior sample preparation. The spectra were measured by placing directly a film of oily sample on the surface of ATR diamond and spectra obtained baseline-corrected and normalized using the zero point at the minimum ordinate value. All FTIR spectra were collected at room temperature at a spectrum resolution of 4 cm^{-1}, with an average of 16 scans over the range from 4000 to 450 cm^{-1}.

2.2.2. Gas chromatography (GC-MS) of CoFA

CoFA samples were methylated with 2wt % H_2SO_4 in water-free methanol at 90°C for 60 min. The fatty acid methyl esters were extracted into heptane and analyzed by gas chromatography/mass spectrometry (Agilent 9000 gas chromatograph system, Intuvo, USA), equipped with an HP-5MS column (30 m × 0.25 mm i.d., and 0.25 μm film thickness) and an Agilent 5975 mass-selective detector. Helium was used as carrier gas at a flow rate of 1 mL/min. The initial temperature of the oven was set at 60°C for 1 min, then to 220°C at a rate of 20°C/min, held for 2 min, and finally to 280°C at 10°C/min, held for 30 min. The compositions of technical OA, LA and CoFA are reported in Table 1.

2.2.3. Differential Scanning Calorimetry (DSC)

Differential scanning calorimetry (DSC) thermograms were recorded on a DSC Mettler-Toledo DSC 3 system under a nitrogen atmosphere. For each DSC run, a sample of weight usually in the range 14-20 mg was hermetically sealed in a standard DSC aluminum crucible pan. The sample was first heated from room temperature to 50 °C (above samples melting temperature) at a heating rate of 2 °C/min and then kept at this temperature for 15 min in the DSC instrument, then cooled to -25 °C, followed by an isothermal segment for 15 min. The second heating scans were run from -25 °C to 50 °C at a heating rate of 2 °C/min followed by a 15 min isothermal segment [27]. This heating-cooling cycle was repeated three times to obtain an acceptable reproducibility [28]. The first cycle was discarded as recommended by Gallart-Sirvent et al. [34], second and third cycles were found identical and thus, the results of the second cycle were reported herein. Prior to measurements, the DSC system was calibrated using indium and zinc.

Table 1
Compositions of technical OA, LA and CoFA.

Fatty acids	CO	CoFA	Technical LA	Technical OA
Caproic (C6:0)	0.13	0.0	0	0
Caprylic (C8:0)	3.15	0.04	0	0
Capric (C10:0)	3.92	2.04	0	0
Lauric (C12:0)	42.96	42.14	0	0
Myristic (C14:0)	21.22	23.02	0	0
Palmitic (C16:0)	12.31	14.36	5	5
Stearic (C18:0)	4.15	4.95	2	2
Oleic (C18:1)	9.74	11.25	25	80
Linoleic (C18:2)	2.43	2.19	67	12

2.2.4. Thermal conductivity of PCMs by transient hot wire method

Thermal conductivity of the fatty acid mixtures was measured according to the standard methods ASTM C1113 and ISO 8894 with some modifications. This technique known as transient hot wire method is used to measure the thermal conductivity of liquids and solids [35]. This implies a particular heat conduction equation that is valid for a linear heat source in a homogenous and isotropic medium at uniform initial temperature [36,37]. The method considers one dimensional radial heat flow inside a homogenous and isotropic test medium. An electrically heated wire is inserted into a sample initially at uniform and constant temperature, and the temperature of the heat source is recorded with respect to time during a brief heating period [35-38]. A schematic illustration of the in-house made apparatus to measure the thermal conductivity of the PCMs is shown in the Fig. 1. The used hot wire was made of Kanthal with 150 mm length and 0.3 mm diameter. Two electrically insulated copper wires with diameter of 2 mm were used to hold the hot wire by welding its ends to the copper wires. A 0-15 volt range D. C power supply was used to supply constant current to the wire (3.3 V, 1.31 A). Voltage and amperage were recorded using a digital multimeter. The temperature was measured with a K-type thermocouple with diameter of 1 mm and accuracy of ±0.1 °C, which is electrically insulated and glued to the wire while the distance between the thermocouple and wire was kept 1 mm. A data logger was used to record temperature versus time with two seconds interval. The sample was placed in a glass tube with a length of 160 mm and a diameter of 20 mm, and then the hot wire set-up was embedded and fixed in the centerline of the tube. Prior to the measurements, the temperature was recorded for 6 sec to make sure there is a constant temperature inside the sample; a switch was then used to run the set-up for 30 sec. The measurements were reproduced five times for each sample and the average results are reported. The temperature-time curve was then transformed to temperature-ln(t) curve and the slope of the new curve in the linear part ($R^2 = 0.99$) is used to calculate the thermal conductivity Eq. (1).

$$\lambda = \frac{V.I.\Delta\ln(t)}{4\pi L.\Delta T} = \frac{V.I}{4\pi L.\left(\frac{\Delta T}{\Delta\ln(t)}\right)}. \quad (1)$$

where λ is the thermal conductivity of the sample; V and I are measured voltage and amperage; ΔT is temperature difference over a known time interval; $\Delta\ln(t)$ is the difference between two taken points on temperature-ln(t) curve; L is the length of hot wire; $\frac{\Delta\ln(t)}{\Delta T}$ is the slope of the temperature-ln(t) curve.

2.2.5. T-history, specific heat capacity and enthalpy

T-history method is used to measure melting/freezing point, latent heat of fusion, degree of super cooling and specific heat capacity of several samples simultaneously [39-44]. The T-history set up used in this study was based on [39,43] with some modification and is shown schematically in Fig. 2 (left). Four PCM samples and ultrapure water as reference were tested simultaneously. Stainless steel tubes (SS316) with internal diameter of 10 mm, 1 mm wall thickness and 150 mm length were used as containers for PCM samples and reference material (Fig. 2 (right)). The containers were filled with PCMs up to 140 mm, while 10 mm was left for possible volume expansion during heating/cooling cycles. The containers are thermally insulated using 10 mm thickness ARMAFLEX insulation material [39,41-43]. K-type thermocouples were

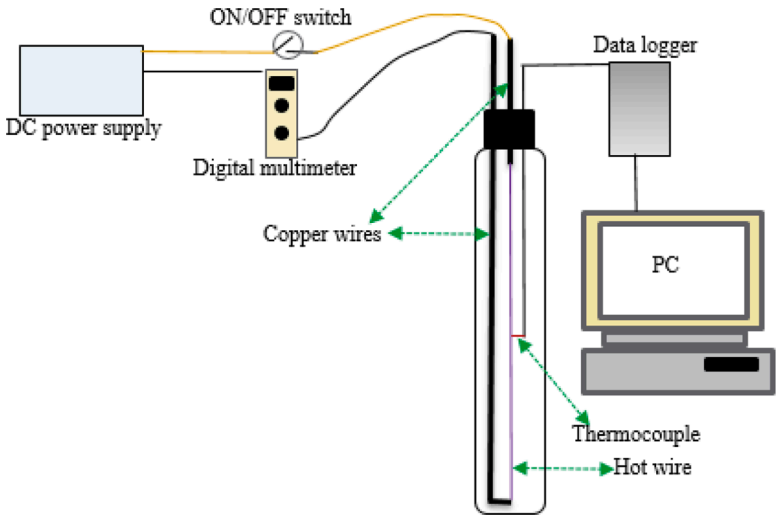

Fig. 1. Schematic diagram of the transient hot wire test set.

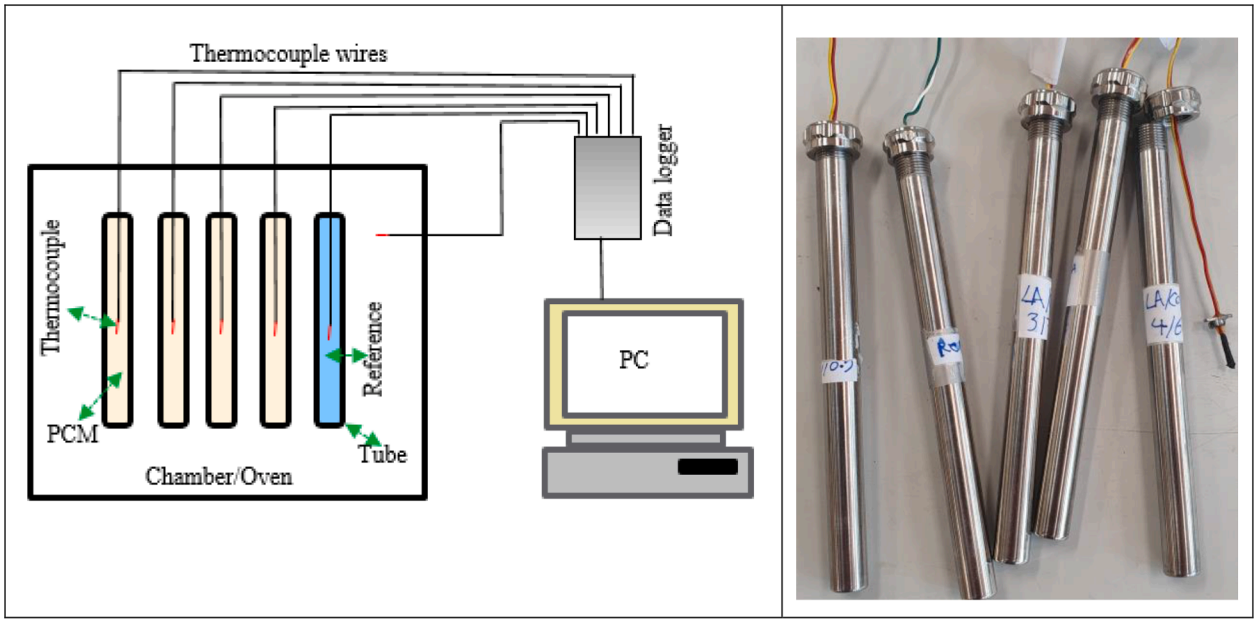

Fig. 2. PCM containers used for T-history experiments (right), and schematic diagram of the set up (left).

used to record temperature changes over time for each sample and reference. The thermocouples were placed at the centerline and in the middle of each container. For cold and hot ambient, two separate chambers were employed, a climate chamber was used as cold ambient fixed at 6 °C, and an oven was used as hot ambient fixed at 40 °C (Fig. 3), the ambient chamber/oven temperatures were recorded with two separate thermocouples. Samples and reference were first preheated in the oven at 40 °C, and then quickly transferred into the climate chamber at 6 °C and the temperature profile was recorded. Once the equilibrium temperature was reached (ca. 2 h), the samples and the reference tubes were transferred into the oven at 40 °C and the temperature changes were recorded. The process (cooling/heating) was repeated twice to verify the reproducibility of the results.

T-history is based on lumped capacitance method, requiring a negligible temperature gradient inside samples during heating/cooling process. This is possible by maintaining a low Biot (Bi) number, expressed in Eq. (2). A low Bi number is reached when the external heat resistance is maintained as high as possible compared to internal heat resistance inside the tube (samples). By using thermal insulation to increase the outer thermal resistance, a Bi number less than 0.1 can be achieved [39]. The thermal resistance of all the heat transfer components contributing to heat transport to/from the material inside the containers are illustrated in Fig. 4. The outer thermal resistance contributes to the outer overall heat transfer coefficient (u), while the internal thermal resistance defined in green color (see Fig. 4) is related to materials inside the tubes. Both the tube and the insulation were considered as outer resistance components. Thus, the outer overall heat transfer coefficient could be described by Eq. 3.

$$\mathrm{Bi} = \frac{u.r}{2.\lambda} \tag{2}$$

where u, r and λ are respectively overall heat transfer coefficient, radius of the container and thermal conductivity of the material.

$$\frac{1}{uA_{tube,in}} = \frac{1}{hA_{ins,out}} + \frac{\ln\left(D_{ins,out}/D_{ins,in}\right)}{2\pi L.\lambda_{ins}} + \frac{\ln\left(D_{tube,out}/D_{tube,in}\right)}{2\pi L.\lambda_{tube}}. \tag{3}$$

where A and D are heat transfer area and tube diameter. Subscribes *tube*

Fig. 3. Samples inside the climate chamber.

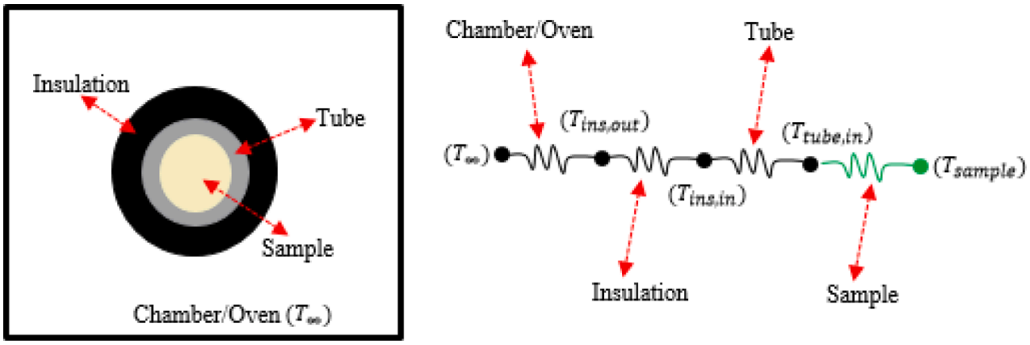

Fig. 4. Cross section schematic diagram of the set-up, with related thermal resistance diagram.

and *ins* refer to the tube container and insulation respectively. h is the convective heat transfer coefficient inside chamber and around samples (insulation body). Subscribes *in* and *out* refers respectively to the inner and outer sides. Internal thermal resistance of main sample is $\delta/\lambda_{pcm}.A_{tube.in}$; δ is characteristics length ($r/2$). The Bi number will be internal thermal resistance per external thermal resistance (Eq. 3), thus the Eq. (2) is obtained.

Energy balance for the reference was considered to obtain overall heat transfer coefficient. The overall heat transfer coefficient (u) for the reference and PCMs are identical since the tubes, thermal insulation and heat transfer condition around them are similar, and according to Eq. (3) these parameters contribute to overall heat transfer coefficient (u). In this study, only the temperature inside the reference and PCMs were recorded and the tubes and the thermal insulation were considered as external thermal resistance, i.e. the energy balance is accepted only for the materials inside the containers. The materials receive/release energy and their temperature changes. As the thermo-physical properties of the reference is known, the amount of energy which is absorbed/released by reference is calculated by Eq. (4) [39,41].

$$Q_{tot} = m.c_p.\left(T_{r,f} - T_{r,o}\right)/\Delta t, \tag{4}$$

where Q_{tot} is the total energy received/released over half a cycle (cooling or heating); m and c_p are respectively the mass and the specific heat capacity of the reference; $T_{r,f}$ and $T_{r,o}$ are final and initial temperatures of the reference; and Δt is the time interval. Since the reference does not undergo phase transition in the considered temperature range, it is possible to consider logarithmic mean temperature difference (LMTD) to obtain the overall heat transfer coefficient (u) as follow:

$$Q_{tot} = uA_{tube,in}.LMTD \tag{5}$$

where LTMD is defined in Eq. (6):

$$LMTD = \frac{\left(T_{r,f} - T_\infty\right) - \left(T_{r,o} - T_\infty\right)}{\ln\left(\frac{\left(T_{r,f} - T_\infty\right)}{\left(T_{r,o} - T_\infty\right)}\right)} \tag{6}$$

where T_∞ is the chamber/oven temperature; Q_{tot} is obtained by Eq. (4). The other temperatures are known, the thermal conductivity determined by transient hot wire, the parameter u is calculated by Eq. (5), and thus, Bi number is calculated.

Specific heat capacity (c_p) of the samples was calculated with the following set of energy balance for reference and PCMs. Eqs. (4) and (5) are equivalent and instead of LMTD it is possible to use the difference between the samples temperature and ambient temperature at each time point. However, by Eq. (5) we obtain overall heat coefficient for the whole half cycle and not at each time point [39,41].

$$m_r.c_{p,r}.\frac{\left(T_r^n - T_{r,o}\right)}{\Delta t} = uA_{tube,in}.\left(T_r^n - T_\infty\right) \tag{7}$$

$$m_{pcm}.c_{p,pcm}.\frac{\left(T^{n}_{pcm}-T_{pcm,o}\right)}{\Delta t}=uA_{tube,in}.\left(T^{n}_{pcm}-T_{\infty}\right) \quad (8)$$

$uA_{tube,in}$ is obtained from Eq. (7) and then substituted in Eq. (8) and by rearrangement, specific heat capacity is obtained as follow:

$$c_{p,pcm}=\frac{m_r.c_{p,r}.\left(T^{n}_{r}-T_{r,o}\right)}{m_{pcm}\left(T^{n}_{pcm}-T_{pcm,o}\right)}.\frac{\left(T^{n}_{pcm}-T_{\infty}\right)}{\left(T^{n}_{r}-T_{\infty}\right)} \quad (9)$$

Enthalpy of the samples is obtained as [39,41]:

$$\Delta H=c_{p,pcm}\left(T^{n}_{pcm}-T_{pcm,o}\right) \quad (10)$$

where ΔH is enthalpy change from initial point to each time point n.

3. Results and discussions

3.1. Visual assessment and selection

In order to design eutectic mixtures with high possible miscibility with the highest possible congruency, theoretical models such as Schröeder-Van Laar approach were employed [45]. However, in this study, the starting material (CoFA) consist of several fatty acids at various proportions (Table 1), thus using theoretical models to predict the eutectic temperatures and the corresponding compositions is not applicable. Therefore, a screening test was conducted to find miscible and stable mixtures, which have phase transition temperature that fits building application. In this regard, the mixtures of LA/CoFA and OA/CoFA (Table 2) were subjected to a visual screening test by exposing the mixtures to temperatures of 5, 15 and 22 °C (Fig. 5) to estimate the phase transition temperatures. The compositions with desirable phase transitions, marked with asterisk (*), were then selected and subjected to further thermal characterization.

Fig. 5 shows phase transition behavior of the mixtures at 5, 15 and 22 °C for LA/CoFA and OA/CoFA mixtures. The screening tests showed that the phase transition temperature of the mixtures increases with increasing the CoFA content. At 5 °C, LA/CoFA compositions with x_{LA}= 0.70 and 0.60, and OA/CoFA compositions x_{OA} = 0.70 are at mushy state, i.e. these compositions have an approximate phase transition around this temperature. LA/CoFA compositions with x_{LA}= 0.50 and 0.45, and OA/CoFA compositions with x_{OA} = 0.60 are at mushy state at 15 °C, while LA/CoFA compositions with x_{LA}= 0.40, 0.35, 0.30 and 0.20 and those of OA/CoFA with x_{OA} = 0.50; 0.45; 0.40 and 0.30 show phase transition at around 22 °C.

3.2. FTIR characterization of CO, CoFA and mixtures

FTIR spectra of refined CO and CoFA at mid region (4000-450 cm^{-1}) is shown in Fig. 6. CO spectrum showed a typical characteristic of absorption bands for triglycerides [46]. The main characteristic vibrations were the stretching vibration of methyl (CH_3) and methylene (CH_2) groups respectively at 2851cm^{-1} and 2919 cm^{-1}, as well as the bending vibrations at 1465 cm^{-1} and 720 cm^{-1}; the C-O stretching vibrations between 1173 and 1104 cm^{-1} and the carbonyl stretching vibrations at 1740 cm^{-1} ($\nu_{C=O}$). Compared to CO, the spectrum recorded for CoFA showed a shift of some absorptions bands, emergence of new and disappearance of others as a result of conversion of the triglyceride ester into carboxylic acid. The prominent shift was observed for the carbonyl stretching vibration at 1707 cm^{-1}, the new absorption bands were observed at 1412, 1284 and 934 cm^{-1} which corresponds to fatty acid O-C stretching vibrations. In addition, the CO vibrations related to triglyceride ester (-C-O) were not found in the CoFA spectrum, thus confirming the complete conversion of CO into CoFA.

Table 2
Primary prepared and selected (*) fatty acid mixtures.

Composition			Composition		
formulation	proportion	x_{LA}	formulation	proportion	x_{OA}
LA/CoFA	70/30	0.7	OA/CoFA	70/30	0.7
LA/CoFA	60/40	0.6	OA/CoFA	60/40	0.6
LA/CoFA	50/50	0.5	OA/CoFA	50/50	0.5*
LA/CoFA	45/55	0.45	OA/CoFA	45/55	0.45*
LA/CoFA	40/60	0.4*	OA/CoFA	40/60	0.4*
LA/CoFA	35/64	0.35*	OA/CoFA	35/65	0.35*
LA/CoFA	30/70	0.3*	OA/CoFA	30/70	0.3
LA/CoFA	20/80	0.2*			
LA/CoFA	10/90	0.1			

To prepare a PCM with transient temperatures in the range of human comfort, the obtained CoFA was mixed with OA and LA at various compositions. The chemical stability of the new PCMs was studied by the ATR-FTIR spectroscopy. Fig. 7 shows the spectra of CoFA, OA, LA, and the mixtures x_{LA} = 0.20 and x_{OA} = 0.30 before thermal cycling. The spectra were similar and displayed the typical vibration bands of fatty acids with the exception of the band at 3008 cm^{-1}, attributed to the cis allylic (C=CH) not observed in the CoFA spectrum, as CoFA consist mostly of saturated fatty acids [47] while OA and LA contains unsaturated fatty acids. This vibration (at 3008 cm^{-1}) could be further used to monitor any chemical changes in the mixture (e.g. rancidification) after thermal cycling.

3.3. Thermal analysis by DSC

Fig. 8 shows the thermal characteristics of CO at various cooling/heating rates. The obtained DSC results showed that CO's transition temperatures are strongly dependent on the cooling/heating scanning rates. The higher cooling/heating rate leads to higher heat flow. During the course of heating, onset and offset temperatures depend on the heating rate, while the peak point remains almost unchanged in all cases. The main variations in temperature could be observed during cooling process, where higher scanning rate leads to lower onset, offset and peak temperatures. Tan and Che Man [48] observed similar behavior when thermal characteristics of CO was studied at a series of heating rates ranging from 1 to 20 °C/min. These results emphasize the importance of T-history method that uses bigger sample size, when the thermal characteristics of the small-scale material depend strongly on the cooling/heating scanning rates. For the studied fatty acids, the cooling/heating rate of 2 °C/min was employed as per recommend in ref. [27].

Fig. 9 shows the DSC curves obtained for CO and CoFA (Fig. 9a), OA and LA (Fig. 9b), OA/CoFA (Fig. 9c) and LA/CoFA (Fig. 9d). In both heating and cooling thermograms of CO (Fig 9a), two overlapping peaks were observed; a small shoulder peak embedded in a principal endothermic/exothermic peak as a result of the difference in the proportion of saturated and unsaturated triacylglycerol (TAG) and fatty acids (FA) [49]. Conversion of CO into free fatty acids (CoFA) resulted in enhancement in its thermal capability as PCM, demonstrated by the higher heat flow, latent heat of fusion (see Table 3), melting and freezing temperatures compared to crude CO. In the heating profile of CoFA (Fig. 9a), a main endothermic peak was observed at 29.7 °C ascribed to the melting point of saturated fatty acids, while the small endothermic peak observed at -11 °C was associated with the melting point of unsaturated fatty acids fraction. The CoFA cooling curve showed almost symmetrical overlapped exothermic peaks attributed to crystallization of the saturated fatty acids and a small peak at -20 °C corresponding to the crystallization of the unsaturated fatty acids proportion.

Compared to CoFA, OA and LA melt and freeze congruently (Fig. 9b), displaying only one broad endothermic peak and one sharp exothermic peak. The melting and freezing points of OA were at 10.8 °C and -2 °C, which is in line with the temperatures range reported in literatures [27, 28]. The small-observed deviation between the present study and the literature data [27,28] in melting and freezing points for OA was mainly

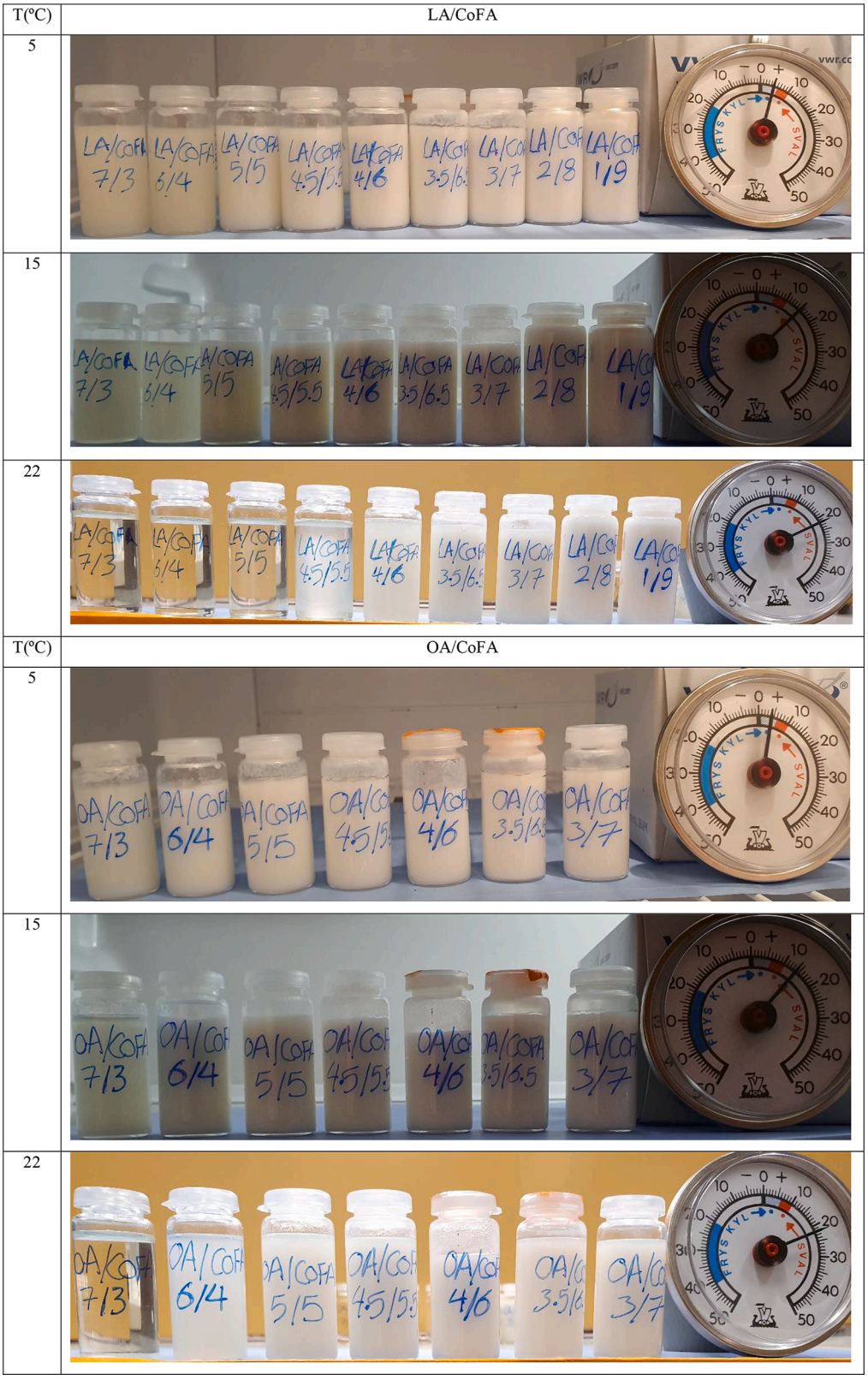

Fig. 5. Primary prepared LA/CoFA and OA/CoFA with different compositions.

attributed to the purity of OA. Indeed, the current study used a technical OA (80%), while Inoue et al. [27,28] employed a pure OA grade. For LA the melting and freezing points were at -10.3 °C and -14.6 °C, which is in agreement with data reported in ref. [50]. OA showed higher phase transition heat flow and latent heat (Table 3) and temperature compared to LA [50].

When OA or LA were mixed with CoFA (Figs. 9c-d), the mixtures showed a tendency of increased phase transition temperatures, heat flow and latent heat of fusion (Table 3) when the amount of CoFA increases in the mixtures. All the mixtures showed two endothermic peak during the

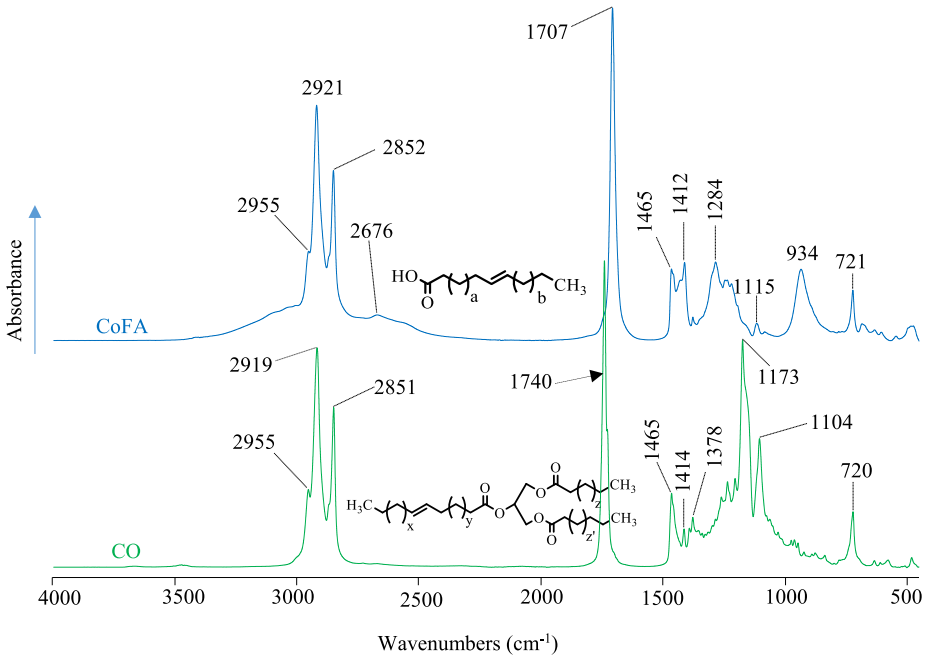

Fig. 6. FTIR absorbance spectra of coconut oil (CO) and coconut oil fatty acids (CoFA).

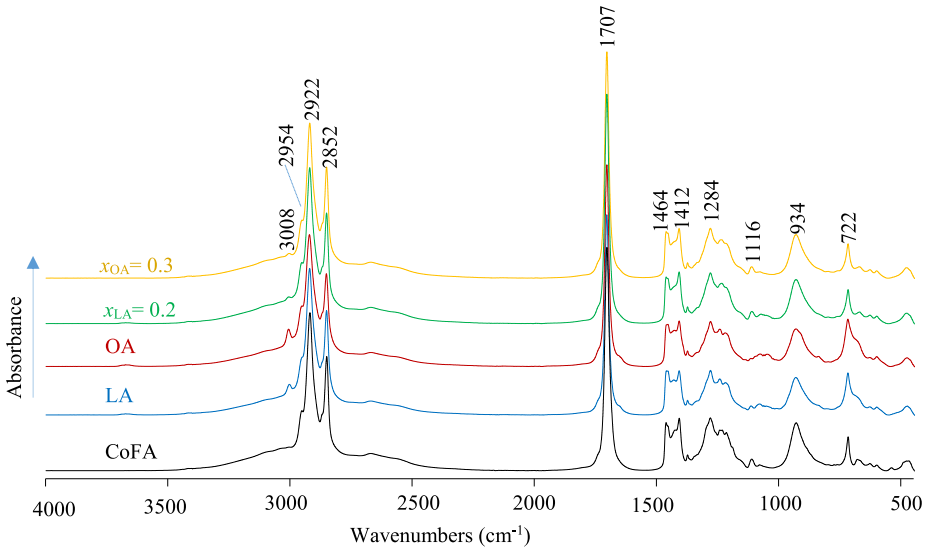

Fig. 7. FTIR absorbance spectra of CoFA, LA, OA, the mixture with x_{LA}= 0.20 and the mixture with x_{OA} = 0.30.

melting process and two exothermic peak in the solidification process, attributed respectively to the melting and freezing points of the fatty acid species in the mixtures. However, the melting and solidification points of the mixtures were higher than the melting and freezing points of the technical fatty acids. In DSC heating thermograms obtained for OA/CoFA mixtures, except the composition x_{OA} = 0.30, all the other mixtures showed a small shoulder embedded in the major endothermic peak at temperatures of 18-22 °C and another sharp endothermic peak at lower temperatures at around -1 °C. The cooling curves also displayed one sharp exothermic peak at temperatures between -13 °C and -15 °C, and a shoulder embedded in major exothermic peak at higher temperatures in the range of 10-22 °C; in all cases the intensity of the peaks change with the decrease of the OA content in the mixtures. Item for the mixtures involving LA, two major endothermic and two exothermic peaks were observed. The exothermic peak at higher temperatures (22 °C) consist of two overlapping peaks in which the intensity of the minor peak decrease as the LA content in the mixture increases, while at lower temperatures (-25 °C) only one sharp exothermic peak was observed. Similar behavior was noticed during heating process. Considering the DSC curves of CoFA (Fig. 9a) and those of the CoFA mixtures (Figs. 9c-d) together, it could be concluded that the observed incongruent freezing behavior was a result of the small incongruency observed for CoFA during freezing process. Although the DSC results of commercial OA showed higher phase transition temperature, heat flow and latent heat of fusion compared to LA, mixtures prepared with LA/CoFA showed higher phase transition heat flow and latent heat of fusion (Table 3). The calorimetric information proved that the mixtures with LA were better in terms of latent heat of fusion and melt congruently compared to those containing OA. Comparable studies [27] involving mixtures of Lauric acid, which is the main fatty acid comprising up to 50% of the refined CO [47], and high purity OA, showed a melting point of mixtures close to that of pure OA and the mixture process leaded to decrease in the

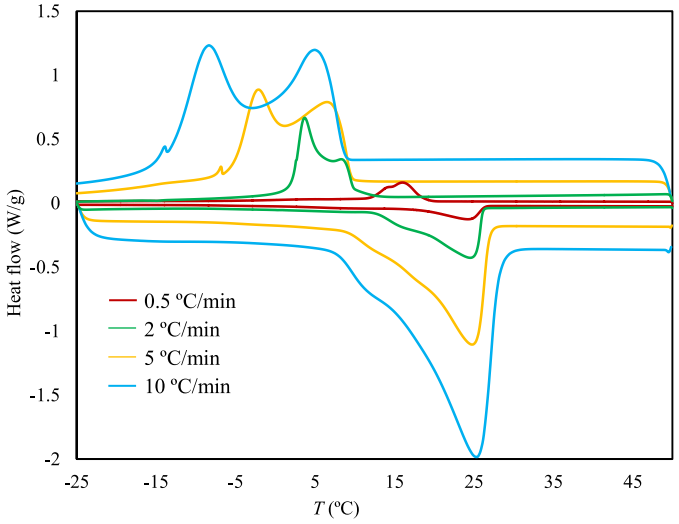

Fig. 8. DSC thermograms of CO at cooling/heating rates varying from 0.5 to 10 °C/min.

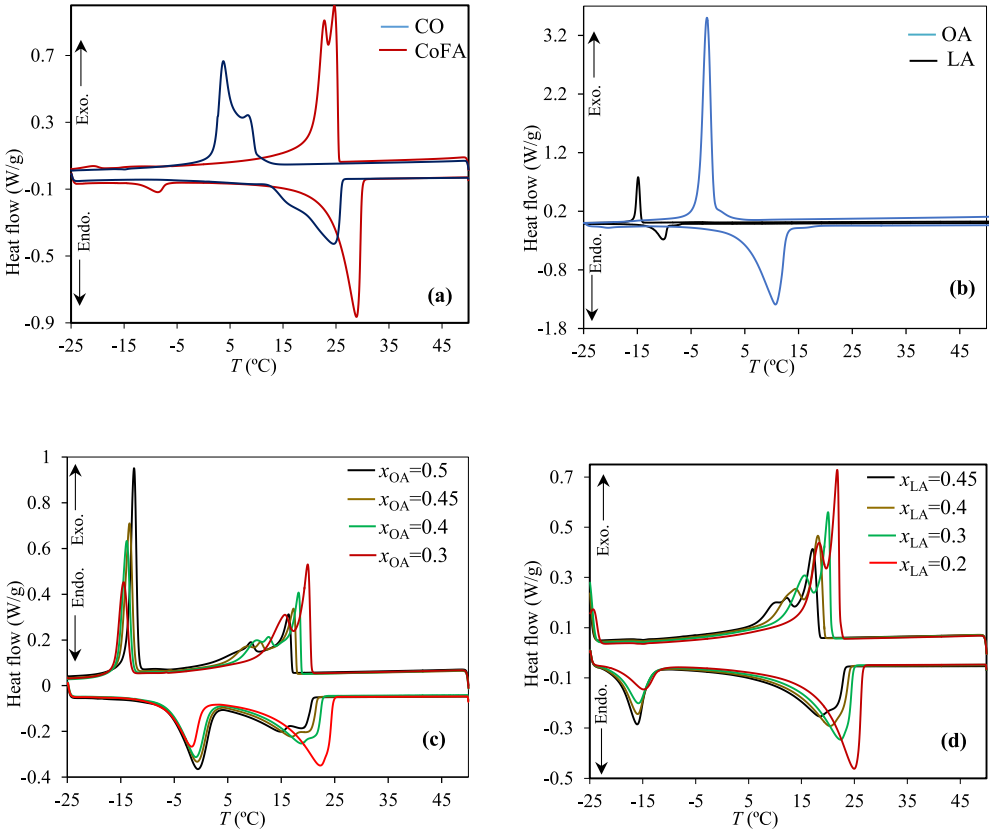

Fig. 9. DSC thermograms obtained for: (a) CO and CoFA, (b) OA and LA, (c) CoFA/OA and (d) CoFA/LA.

melting point of OA as seen in the present study.

In DSC study, temperatures at onset, peak points and end temperatures were reported. The materials start to melt and freeze at T_{onset} (melting/freezing temperatures) and at this temperature; the materials are in mushy state. In order to reach the highest possible absorbing/realizing energy in the considered range, the materials should meet their melting/freezing peak point at the favorable range, and thus peak point was reported through the study. The phase transition temperatures and the enthalpy of fusion are reported in Table 3.

From Table 3 and Fig. 8, CoFA starts to melt at 23.9 °C, a temperature in the target range; however, its melting peak point occurs at 28.5 °C, little outside the suitable temperature range. Thus, it is important to adjust the phase transition behavior of CoFA by mixing it with other fatty acids. In this study, commercial OA and LA were selected and mixed with CoFA to adjust the phase transition temperature of the mixtures. Furthermore, both commercial fatty acids have lower phase transition temperatures and when mixed with the main material, if any incongruency is supposed to happen, it will occur at temperatures far below the target working temperature range.

Table 3
Phase transition temperatures of the PCMs with DSC.

PCMs	Freezing process			Melting process			ΔH_{fusion} (J/g)
	T_{onset}(°C)	T_{peak}(°C)	T_{endset}(°C)	T_{onset}(°C)	T_{peak}(°C)	T_{endset}(°C)	
OA	-0.7	-2	-3.4	4.5	10.8	12.73	93
LA	-14.2	-14.6	-15.5	-12.5	-10.3	-9.3	85.5
CO	6.7	4; 8	2.2	14.5	24.4	26.1	100
CoFA	25.6	23; 25.6	21.1	23.9	28.5	29.8	122.7
$x_{OA} = 0.50$	16.6	16.5	5	7	18.9	20.8	34
$x_{OA} = 0.45$	18	17.5	5	8.7	17	25.6	41
$x_{OA} = 0.40$	18.9	18.4	5	10.5	18.8	22.7	49
$x_{OA} = 0.30$	20.6	15; 20.2	8.8	14.4	22.2	24.7	63
$x_{LA} = 0.40$	18.4	17.3	14.4	8.8	18.4	23.2	63
$x_{LA} = 0.35$	19.4	13.8; 18.3	7.3	11.3	20.3	24.2	70.4
$x_{LA} = 0.30$	20.7	15.7; 20.2	10.2	13.8	22.3	24.8	77.3
$x_{LA} = 0.20$	22.4	22; 18.5	14.7	17.5	24.8	26.5	94

3.4. Thermal conductivity measurement with transient hot wire

Fig. 10 exemplifies the temperature-ln(t) profiles obtained from transient hot wire experiments measured in both solid and liquid states for $x_{LA} = 0.20$ and ultrapure water. Before each measurement, the experiment set up was calibrated using pure water, which showed a mean value of 0.597 W/m K, and is in an agreement with the reference value of 0.6 W/m K [51]. The segment (10 sec) of the graph where there is a linear trend, with higher R^2 >0.99, was selected to calculate the thermal conductivity using the Eq. (1). The results are reported in Table 4 where the values are means of five measurements.

The thermal conductivity values of the tested mixtures were around 0.2 W/m K for samples at liquid state and around 0.35 W/m K, at solid state. The thermal conductivities of mixtures at liquid state were comparable to those of individual fatty acids and no relationship was found between the mass fraction of OA or LA in the mixtures and the thermal conductivity. The reproducibility of the experiments was acceptable as demonstrated by the low standard deviation values. The experimental uncertainty due to measurement instrument including thermocouple, caliper and multimeter was determined and found to be 1.92%. The details of the calculations are given in the experimental uncertainty analysis section.

3.5. Thermal analysis with T-history

T-history method requires a negligible temperature gradient inside the samples to fulfil the lumped capacitance assumption, which achieved when Bi number is small (Bi<0.1) [39]. As the thermal conductivity was determined to be around 0.2 W/m K, and the overall heat transfer coefficient of 5.13 W/m^2 K, was calculated Eqs. 4-(6), the Bi number was found to be 0.06 (Eq. (2)), i.e. satisfying the considered assumption.

Table 4
Average thermal conductivity of materials with standard deviation in parentheses.

Samples	Mean λ (W/m K)	
	Liquid	Solid
Water	0.597 (0.016)	-
OA	0.206 (0.010)	-
LA	0.196 (0.013)	-
CO	0.200 (0.016)	-
CoFA	0.21 (0.007)	0.351 (0.015)
$x_{OA} = 0.50$	0.212 (0.004)	0.357 (0.010)
$x_{OA} = 0.45$	0.202 (0.004)	0.355 (0.011)
$x_{OA} = 0.40$	0.192 (0.009)	0.357 (0.008)
$x_{OA} = 0.30$	0.216 (0.014)	0.39 (0.007)
$x_{LA} = 0.40$	0.192 (0.005)	-
$x_{LA} = 0.35$	0.212 (0.007)	0.36 (0.03)
$x_{LA} = 0.30$	0.191 (0.001)	-
$x_{LA} = 0.20$	0.202 (0.011)	0.346 (0.012)

Fig. 11 shows T-history profiles for CO, CoFA and water as reference. The figure shows that CO undergoes a large supercooling (around 2.5 °C), while this is negligible for CoFA. CO cools down to 17.6 °C, the temperature at which supercooling occurs, then the temperature goes up to 20 °C, which is the solidification temperature. During heating process,

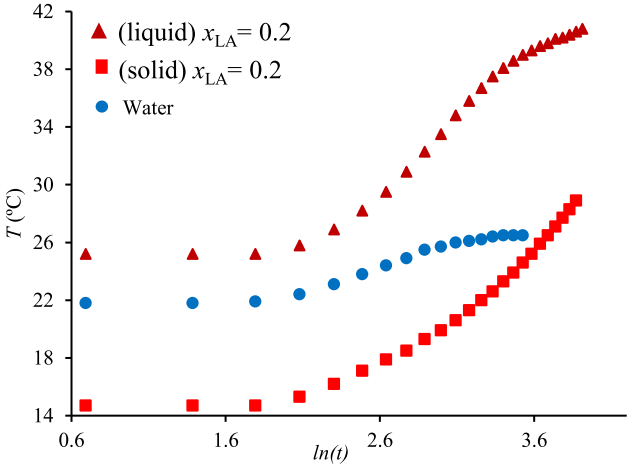

Fig. 10. Temperature-ln(t) profiles of tested sample $x_{LA} = 0.20$, in a solid and liquid states and water.

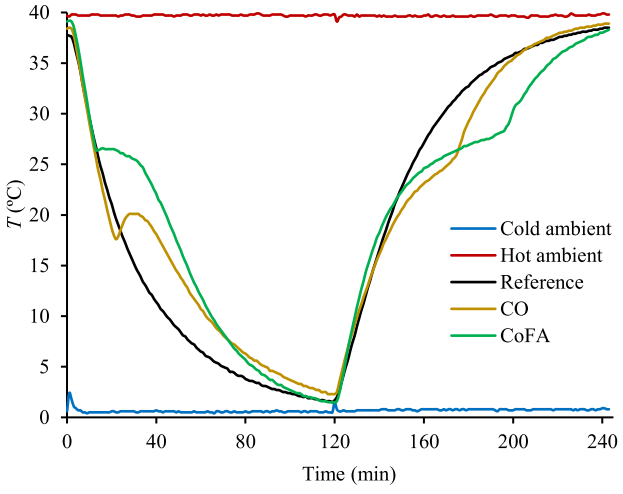

Fig. 11. T-history over cooling/heating cycle for CO, CoFA and water (reference).

CO starts to melt at temperature around 21 °C, and is fully melted at 26.4 °C. The solidifying temperature for CoFA is 26.4 °C, and it starts to melt at 23.7 °C fully melted at 28.3 °C. For both cooling and heating process, during phase transition, the profile for CoFA is wider than that of CO indicating that CoFA can store and release more energy compared to CO.

Fig. 12 shows the T-history profile for LA/CoFA (Fig. 12a) and OA/CoFA (Fig. 12b) mixtures over two heating/cooling cycles. Ultrapure water was used as reference, and the measured ambient temperatures were constant throughout the experiments with ± 0.8 °C maximum deviation. Once placed in the climate chamber at 6 °C, the test samples and reference temperatures decrease gradually from the starting temperature at 40 °C and continues to decease with the time until it reaches the chamber's ambient temperature (6 °C). During the course of cooling cycles, a phase change transition was observed for all the mixtures between the temperature ranges from 21.3 to 17.6 °C for OA/CoFA and from 23.1 to 19.6 °C for LA/CoFA mixtures. When the cooling process continued, some mixtures experienced a second solidification point around 18 and 12.5 °C for OA/CoFA and between 19 and 14.5 °C for LA/CoFA mixtures. Small subcooling effect, less than 0.6 °C, was observed in all cases. During heating cycles, only one phase transition was noticed for each mixture, which means the mixtures melt congruently. The melting temperature ranges were found around 19.6 to 23.1 °C for OA/CoFA and between 20.7 and 25.5 °C for LA/CoFA mixtures. A deviation of all the formulations curves from the reference curve was noticed when the temperature profiles approaches the cold (6 °C) or hot ambient temperature (40 °C) probably due to differences in thermal conductivity.

Enlargement of the heating/cooling curves in the phase transition regions (Fig. 13), showed that above phase transition, mixtures tend to deviate and increment forehead than others, indicating a greater heat capacity of some mixtures than the others. These increments were found to increase with the increase of CoFA content in the mixtures. Furthermore, compositions with high CoFA content experienced higher phase transition temperature than those with low CoFA content (Fig. 13).

Fig. 14 shows the specific heat capacity and the enthalpy for OA/CoFA and LA/CoFA mixtures calculated using Eqs. (9) and (10) during cooling and heating processes. The calculated heat capacity OA/CoFA (Fig. 14a) is in the range of 0.5-3.5 J/g K, and for LA/CoFA (Fig. 14b) is in the range of 0.9-5.5 J/g K (during phase transition). For both mixture types, the heat capacity tends to increase when the portion of CoFA increases in the compositions. During cooling process, due to incongruent freezing and small degree of subcooling, there is certain inevitable difficulties in interpreting the C_p. However, as it is seen from the figures, super cooling effect was small, and it has no significant effect on the measured C_p. Fig.s 14c and 14d respectively show enthalpy for OA/CoFA and LA/CoFA mixtures for cooling and heating process during the

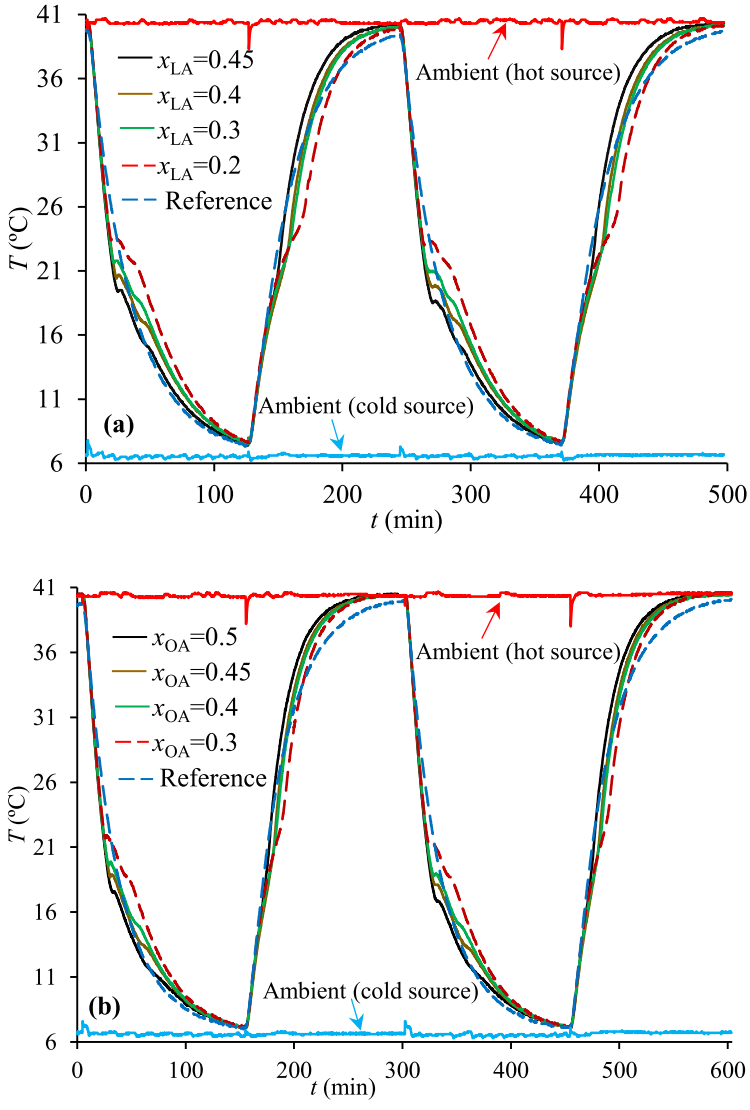

Fig. 12. T-history over two heating/cooling cycles for (a) LA/CoFA and (b) OA/CoFA mixtures.

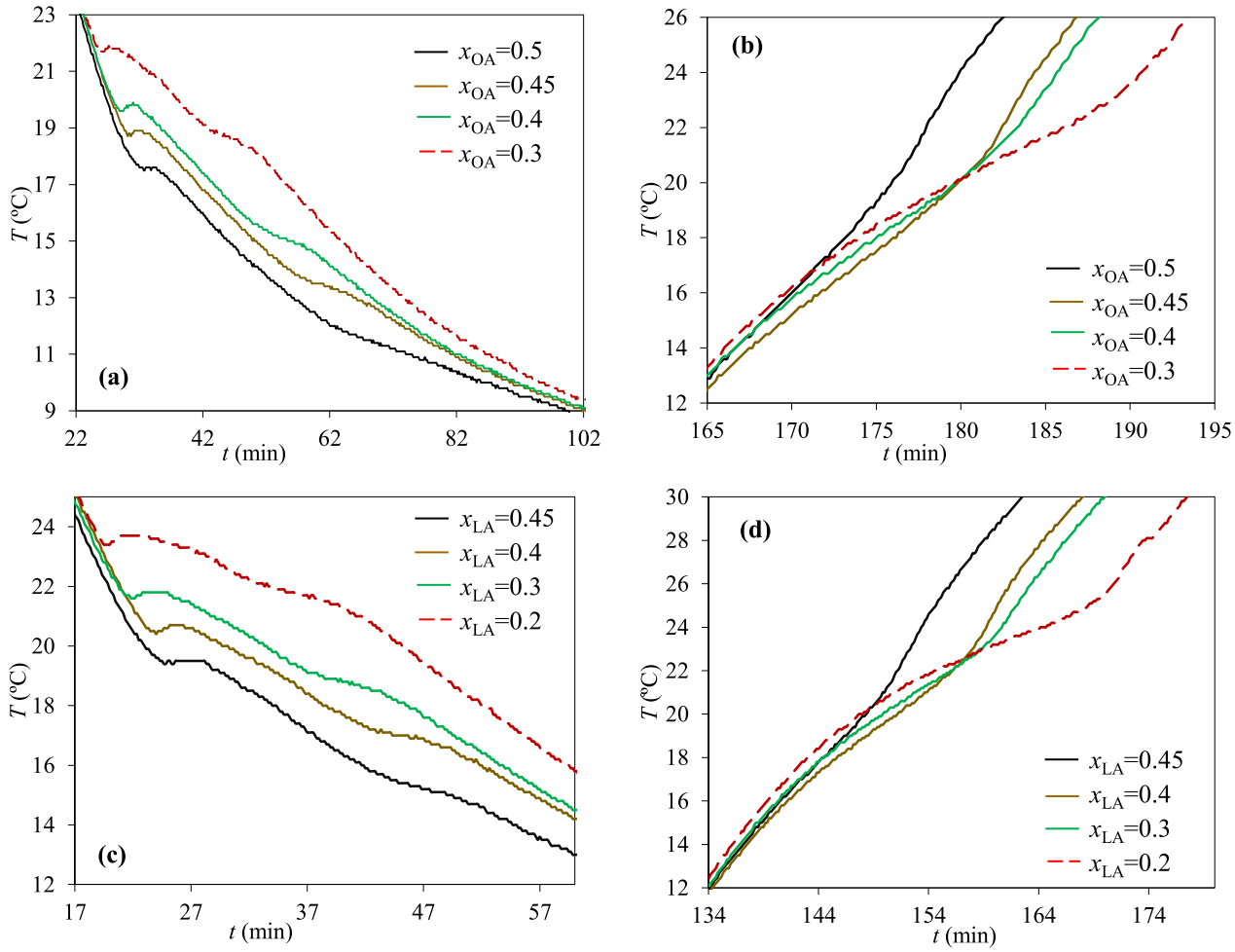

Fig. 13. T-history curves enlargements in the transition regions during cooling (a,c) and heating process (b,d) for OA/CoFA and LA/CoFA mixtures.

first cycle calculated by Eq. (10). The values of cooling process are negative, i.e. the samples released energy while the values are positive during heating since the samples absorb energy. The effect of inevitable incongruent phase transition during cooling process is observed likewise C_p and even an effect of super cooling can be seen. Phase transition temperatures, melting/freezing C_p and enthalpy are tabulated in Table 5.

Due to incongruent freezing during cooling process, two different transition temperatures were observed, as a consequence, part of energy is released in the form of sensible energy, thus explaining the difference between the values for cooling and heating for C_p and enthalpy (Table 5). From the result, $x_{LA} = 0.20$ can be selected as the most promising material, since it absorbs and releases more energy compared to other materials in the studied temperature range. Moreover, its heat capacity is considerably higher than of the other mixtures. Within the OA/CoFA group, the mixture with composition with $x_{OA} = 0.30$ shows best properties. However, LA/CoFA mixtures show better performance.

3.6. Comparison between DSC and T-history

DSC and T-history methods were used to compare the thermophysical properties of the OA/CoFA and LA/CoFA mixtures. Compared to DSC experiments, which require very small amounts of sample with rapid response times, T-history uses larger amount of samples comparable to the real applications of the PCMs [44]. Moreover, DSC results are dependent on the cooling/heating rates, in particular during cooling process, thus T-history method gives more reliable results. T-history results indicated that all the tested combinations displayed a super cooling phenomenon, which was not evident from the DSC results (Figs. 9a-d). A comparison of the phase transition temperatures and enthalpies calculated from DSC and from T-history is summarized in Table 6. The results indicated that for samples having less or no incongruent melting, the determined melting peak points from the both methods were comparable. However, due to the incongruent freezing and super cooling observed during cooling process, the determined results from the two methods were slightly different but still in a reasonable agreement. Table 6 also shows the calculated enthalpy for fatty acid mixtures obtained by T-history and DSC methods. The results support the conclusion that compositions with congruent phase transitions, both methods provide comparable results; however, the difference in calculated enthalpies between the methods is greater for compositions undergoing super cooling and incongruency during cooling process.

Small difference in sub-cooling effect has been observed between DSC and bulk sample T-history method. Calculation of enthalpy gives more insight of PCM thermal energy storage and and discharge capacity and design of the storage system. However, for the comparison of PCM properties and considering the operating temperature for maximum energy storage and discharge, evaluation of PCM enthalpy is essential. DSC and T-history study's outcome indicates that $x_{LA} = 0.20$ has the largest enthalpy and heat capacity and an operating temperature in the range of 18-25°C, which makes it a promising candidate for using as BPCM for building applications.

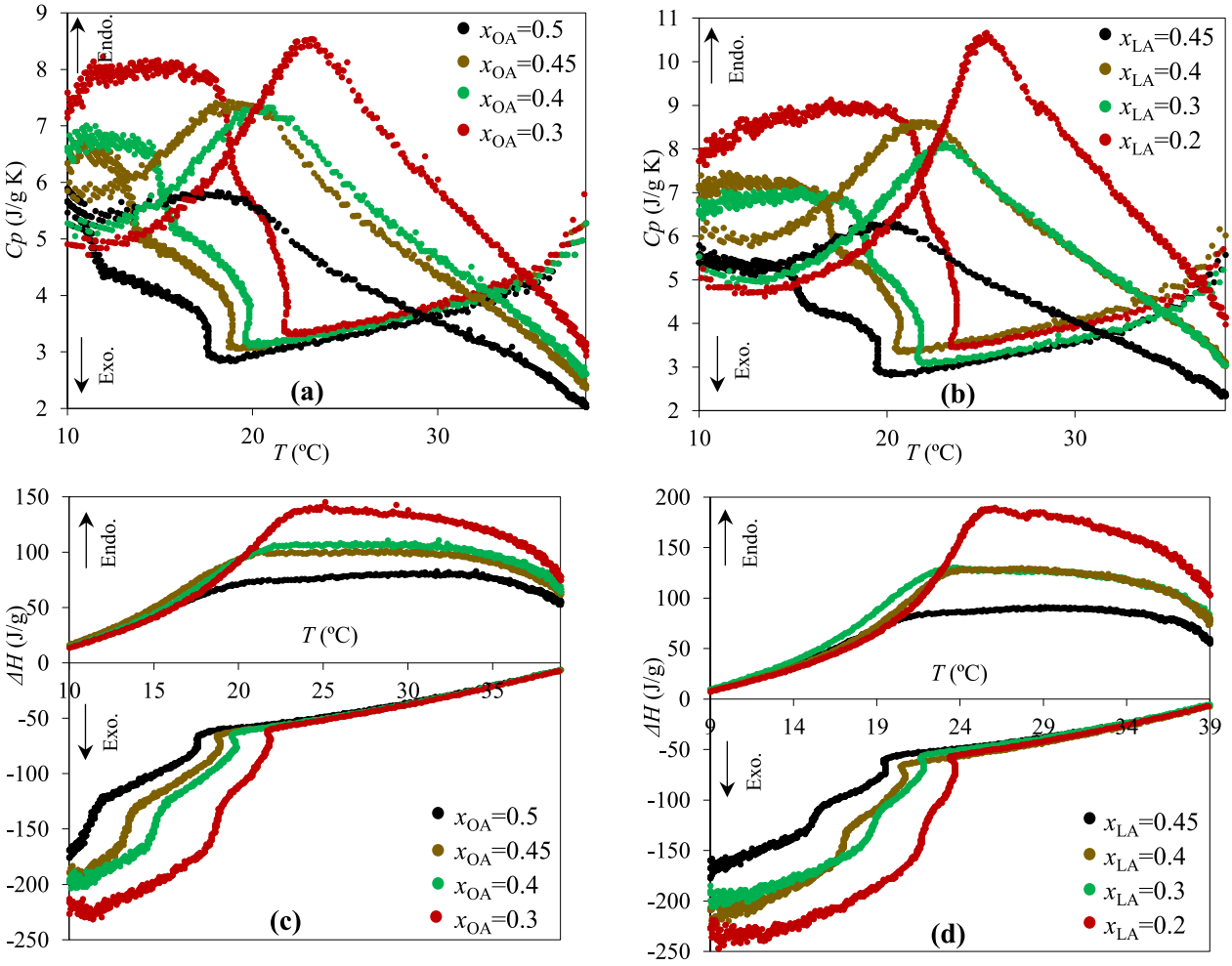

Fig. 14. Melting and freezing specific heat capacity for (a) OA/CoFA and (b) LA/CoFA mixtures, and enthalpy for (c) OA/CoFA and (d) LA/CoFA.

Table 5
Thermal properties of the samples obtained by T-history.

Samples	T (°C)		C_p (J/g K)		ΔH (J/g)	
	Freezing	Melting	Freezing	Melting	Freezing	Melting
x_{OA} = 0.50	11.9; 17.4	19.6	0.7; 1.4	0.5	16; 44	38
x_{OA} = 0.45	13.2; 18.8	20.7	0.8; 1.6	1.63	17; 37	49
x_{OA} = 0.40	15; 19.7	21	0.8; 1.6	1.95	16; 42	53
x_{OA} = 0.30	18.6; 21.7	23.1	1.6; 2	3.5	21; 43	76
x_{LA} = 0.40	15.3; 19.5	20.7	0.8; 1.2	0.9	16; 29	51
x_{LA} = 0.35	17; 20.6	22.5	1; 1.6	2.7	23; 37	67
x_{LA} = 0.30	18.8; 21.8	23.1	1.3; 1.6	3	20; 40	73
x_{LA} = 0.20	21.7; 23.7	25.5	2.3; 2.8	5.5	24; 54	104

3.7. Accelerated thermal cycling

Samples were subjected to an accelerated thermal cycling to access the thermal stability of BPCMs. Accelerated cooling/heating cycles in most cases are carried out from 100 to 1000 cycles [52-57]. In this work an accelerated thermal cycling test with 700 cooling/heating cycles was performed in a climate chamber oscillating between -3 to 50 °C, at heating and cooling rates of 2 °C/min, with 10 min isothermal segment at -3 °C and 50 °C. The temperature range (-3 to 50 °C) and isothermal segments were selected to ensure a complete solidification and melting of the PCM during a cycle. For each composition, five vials with 2 g PCM each were prepared, sealed and placed in a climate chamber for thermal cycling. After each 100th cycle, a vial from each composition was taken for chemical (FTIR) and thermal (DSC) characterization. By prompting clarity, only the results of the composition $x_{LA} = 0.20$ were reported. The obtained DSC curves of $x_{LA} = 0.20$ subjected to 100, 200, 300, 400 and 700 thermal cycles are shown in Fig. 15. After 100 heating /cooling cycles, the DSC curves of the studied PCMs showed identical exothermic and endothermic peaks as before cycling process in terms of shape; however a slow shift (ca. 0.2°C) to lower temperatures were observed during both melting and solidification processes. No relationship was observed between the number of thermal cycles and the changes in phase transition temperatures. Thermal cycling resulted also in a small reduction in solidification heat flow, while the melting heat flow remained almost unchanged. These changes in phase transition temperatures and heat flows were below 1% even after 700 heating/cooling cycles, indicating that the material has very good thermal cycling stability. The changes in phase transition temperatures (melting/solidification) as well as the heat flows losses after thermal cycling is common phenomenon when mixtures of fatty acid were studied [58,59]. Fauzi et al. [58] reported that the changes of melting point of myristic acid/palmitic acid and myristic acid/palmitic acid/sodium stearate eutectic mixtures were irregular but of acceptable magnitude, and a

Table 6
Phase transition temperature and enthalpy comparison between T-history and DSC.

Samples	Freezing point T (°C)		Melting point T (°C)		Freezing enthalpy (J/g)		Melting enthalpy (J/g)	
	T-history	DSC	T-history	DSC	T-history	DSC	T-history	DSC
$x_{OA} = 0.50$	11.9; 17.4	9.8; 16.5	19.6	15.5; 18.9	16; 44	48.8	38	34
$x_{OA} = 0.45$	13.2; 18.8	11.3; 17.5	20.7	17; 20.4	17; 37	55.1	49	41
$x_{OA} = 0.40$	15; 19.7	13.3; 18.4	21	18.8	16; 42	53.2	53	49
$x_{OA} = 0.30$	18.6; 21.7	15; 20.2	23.1	22.2	21; 43	70.1	76	63
$x_{LA} = 0.40$	15.3; 19.5	13; 17.3	20.7	18.4	16; 29	68.5	51	63
$x_{LA} = 0.35$	17; 20.6	13.8; 18.3	22.5	20.3	23; 37	75.7	67	70.4
$x_{LA} = 0.30$	18.8; 21.8	15.7; 20.2	23.1	22.3	20; 40	80.7	73	77.3
$x_{LA} = 0.20$	21.7; 23.7	18.5; 22	25.5	24.8	24; 54	92.8	104	93

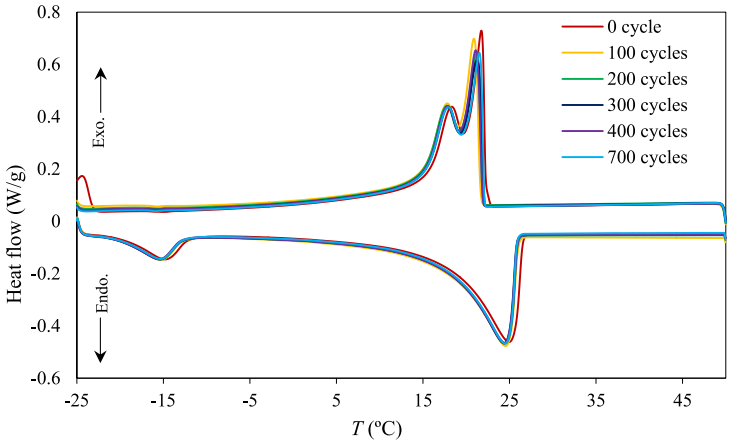

Fig. 15. DSC curves of $x_{LA} = 0.20$ subjected to long-term thermal cycles.

decrease between 6 and 10.1% in latent heat of fusion were observed after 1500 cycles. A study on thermal stability of a composite made of palmitic acid/stearic acid eutectic mixture as PCM and expanded graphite was performed by Zhang et al. [59] reported a loss below 3% in melting and solidification enthalpies after 720 thermal cycles. Thus, the observed changes in thermal properties such as melting temperatures and latent heat of fusion of LA/CoFA mixture are in agreement with the literature and constitute reliable BPCM for thermal energy storage in building applications.

Changes in phase transition temperatures and enthalpy lost of PCMs after thermal cycling are caused by the degradation of PCM components, and/or presence of impurities in the fatty acids used in preparation of

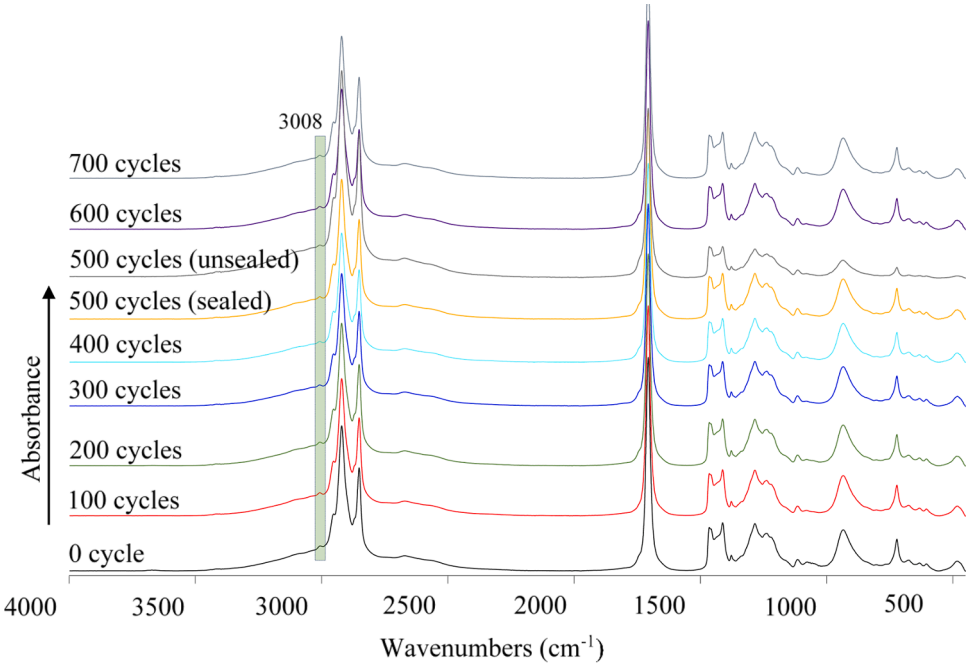

Fig. 16. FTIR spectra of $x_{LA} = 0.20$ before and after long-term thermal cycles.

the mixtures [58-63]. In this study, the physical appearance of the studied mixtures after 700 cycles remained unchanged. To prove the chemical stability of the mixtures, sealed and unsealed samples were analyzed by FTIR before and after thermal cycling and the obtained spectra are shown in Fig. 16 (only the spectra of the mixture $x_{LA} = 0.20$ were reported). The samples subjected to thermal cycling showed the same characteristic absorption peaks as the uncycled sample, namely vibrations at 2954, 2922, 2852, 1707, 1464, 1412, 1284, 1116, 934 and 722 cm^{-1}. All the absorption peaks remained at the same frequency band and have the same intensities, and there is no appearance or disappearance of peaks, indicating that the chemical structure of the mixture was not altered during the thermal cycling. This result was corroborated by the physical appearance of samples, which did not change after thermal cycles. Thus, the observed shifts in phase transition temperatures and loss in enthalpy, after heating/cooling cycles, was not caused by the chemical structure degradation but rather by the presence of impurities in the commercial LA and synthesized CoFA. Similar results were reported in the literature when fatty acid binary and tertiary mixtures were subjected to long-term thermal cycles [58,60,63,64].

Pure LA is a polyunsaturated fatty acid; it is susceptible to oxidation when exposed to air, humidity and temperature. In order to assess the chemical stability of the LA and LA/CoFA mixtures during thermal cycling, unsealed samples of LA and $x_{LA} = 0.20$ were subjected to thermal cycling process likewise sealed samples. DSC and FTIR results after 500 cycles showed no differences between sealed and unsealed samples. The unchanged vibration at 3008 cm^{-1} (Fig. 16), confirms the thermal and chemical stability of the mixture.

4. Experimental uncertainty analysis

Experimental uncertainty associated with the thermal conductivity measurements by transient hot wire, specific heat capacity and enthalpy by T-history are introduced by the combination of the experimental errors, the calculations error and the accuracy of the measurement tools. In the current study, the overall errors were related to thermocouples, multimeter used to measure electrical voltage and current, balance to measure weight of the samples, and the caliper to measure the lengths. The uncertainty of the thermocouple is ± 0.1 °C, that of multimeter is ± 0.01 V, and that of balance and caliper are respectively 0.0000002 kg, and 0.00002 m. The uncertainty analysis was calculated using Kline and McClintock method [65]. The uncertainty is calculated by using Eq. (11).

$$U_R = \left[\sum_{i=1}^{n}\left(\frac{\partial R}{\partial P_i}U_{P_i}\right)^2\right]^{\frac{1}{2}}, 1 \le i \le n \quad (11)$$

where R and P_i are dependent and independent variables respectively. U_R and U_{P_i} are the uncertainties for the dependent and the independent variables respectively. The non-dimensional form of Eq. (11) is $\left(\frac{U_R}{R}\right) \times 100$) which is in percentage [65-67]. The independent measured variables used to calculate the experimental uncertainties were summarized in Table 7.

Table 7
Measured variables, experimental uncertainties and specifications of the used equipment.

Measured variable	Nomenclature	Nomenclature of uncertainty	Nominal value	Absolut uncertainty
Voltage	V	U_V	3.3 V	0.01 V
Amperage	A	U_I	1.31 A	0.01 A
Mean ΔT in hot wire	T	U_T	6 °C	0.1 °C
Length of hot wire	L	U_L	0.15 m	0.00002 m
Maximum $(T_r^n - T_{r,i})$ in T-history	T	U_T	33 °C	0.1 °C
Maximum $(T_{pcm}^n - T_{pcm,i})$ in T-history	T	U_T	33 °C	0.1 °C
Maximum $(T_{pcm}^n - T_\infty)$ in T-history	T	U_T	33 °C	0.1 °C
Maximum $(T_r^n - T_\infty)$ in T-history	T	U_T	33 °C	0.1 °C
Average mass of samples	m	U_m	0.009 kg	0.0000002 kg
Average mass of reference	m	U_m	0.01 kg	0.0000002 kg

4.1. Thermal conductivity uncertainty calculation

Based on Eqs. (1) and (11), it is possible to calculate the uncertainties of thermal conductivity using the following Eq. (12):

$$U_\lambda = \left[\left(\frac{\partial \lambda}{\partial V}U_V\right)^2 + \left(\frac{\partial \lambda}{\partial I}U_I\right)^2 + \left(\frac{\partial \lambda}{\partial \Delta T}U_T\right)^2 + \left(\frac{\partial \lambda}{\partial L}U_L\right)^2\right]^{1/2}, \quad (12)$$

where, U_V, U_I, U_L and U_T are respectively the uncertainty for multimeter, caliper and thermometer (Table 7). The uncertainty related to time was assumed to be zero. By applying some mathematical calculations, the Eq. (12), evolve into;

For Δln(t), the value of 0.54 was considered and the mean nominal value of 0.2 W/m K, was considered to normalize the uncertainty of the thermal conductivity. By using Table 7 values in Eq. (13), and after

$$U_\lambda = \left[\left(\frac{I.\Delta\ln(t)}{4\pi L.\Delta T}U_V\right)^2 + \left(\frac{V.\Delta\ln(t)}{4\pi L.\Delta T}U_I\right)^2 + \left(\frac{V.I.\Delta\ln(t)}{4\pi L}.\frac{1}{\Delta T^2}U_T\right)^2 + \left(\frac{V.I.\Delta\ln(t)}{4\pi.\Delta T}.\frac{1}{L^2}U_L\right)^2\right]^{1/2} \quad (13)$$

normalization ($\left(\frac{U_R}{R}\right) \times 100$), the uncertainty associated with the measuring instruments used to determine thermal conductivity was found to be 1.92%.

4.2. Enthalpy and C_p uncertainty calculation

Similar approach used for thermal conductivity uncertainty was adopted to calculate the specific heat capacity and enthalpy uncertainties. For this, uncertainty of the heat capacity for reference (water) was assumed to be zero and the nominal value was 4.189 J/g K. Considering Eqs. (9) and (10) together with Eq. (11), the uncertainty for C_p and ΔH are expressed respectively as follow:

$$U_{c_p} = \left[\left(\frac{\partial c_p}{\partial m_r}U_m\right)^2 + \left(\frac{\partial c_p}{\partial m_{pcm}}U_m\right)^2 + \left(\frac{\partial c_p}{\partial\left(T_r^n - T_{r,i}\right)}U_T\right)^2 + \left(\frac{\partial c_p}{\partial\left(T_{pcm}^n - T_{pcm,i}\right)}U_T\right)^2 + \left(\frac{\partial c_p}{\partial\left(T_{pcm}^n - T_\infty\right)}U_T\right)^2 + \left(\frac{\partial c_p}{\partial\left(T_r^n - T_\infty\right)}U_T\right)^2\right]^{1/2}, \tag{14}$$

$$U_{\Delta H} = \left[\left(\frac{\partial \Delta H}{\partial c_{p,pcm}}U_{c_p}\right)^2 + \left(\frac{\partial \Delta H}{\partial\left(T_{pcm}^n - T_{pcm,i}\right)}U_T\right)^2\right]^{1/2} \tag{15}$$

After mathematical operation, the following Eqs. (16) and (17) are obtained:

$$U_{c_p} = \left[\left(\frac{c_{p,r}.\left(T_r^n - T_{r,i}\right)}{m_{pcm}\left(T_{pcm}^n - T_{pcm,i}\right)}.\frac{\left(T_{pcm}^n - T_\infty\right)}{\left(T_r^n - T_\infty\right)}U_m\right)^2 + \left(\frac{m_r.c_{p,r}.\left(T_r^n - T_{r,i}\right)}{\left(m_{pcm}\right)^2\left(T_{pcm}^n - T_{pcm,i}\right)}.\frac{\left(T_{pcm}^n - T_\infty\right)}{\left(T_r^n - T_\infty\right)}U_m\right)^2 + \left(\frac{m_r.c_{p,r}}{m_{pcm}\left(T_{pcm}^n - T_{pcm,i}\right)}.\frac{\left(T_{pcm}^n - T_\infty\right)}{\left(T_r^n - T_\infty\right)}U_T\right)^2 + \left(\frac{m_r.c_{p,r}.\left(T_r^n - T_{r,i}\right)}{m_{pcm}\left(T_{pcm}^n - T_{pcm,i}\right)^2}.\frac{\left(T_{pcm}^n - T_\infty\right)}{\left(T_r^n - T_\infty\right)}U_T\right)^2 + \left(\frac{m_r.c_{p,r}.\left(T_r^n - T_{r,i}\right)}{m_{pcm}\left(T_{pcm}^n - T_{pcm,i}\right)}.\frac{1}{\left(T_r^n - T_\infty\right)}U_T\right)^2 + \left(\frac{m_r.c_{p,r}.\left(T_r^n - T_{r,i}\right)}{m_{pcm}\left(T_{pcm}^n - T_{pcm,i}\right)}.\frac{\left(T_{pcm}^n - T_\infty\right)}{\left(T_r^n - T_\infty\right)^2}U_T\right)^2\right]^{1/2}, \tag{16}$$

$$U_{\Delta H} = \left[\left(\left(T_{pcm}^n - T_{pcm,i}\right)U_{c_p}\right)^2 + \left(c_{p,pcm}U_T\right)^2\right]^{1/2} \tag{17}$$

By replacing the variables in Eq. (16) with the values in Table 7, the heat capacity uncertainty (U_{c_p}) was found to be 0.02821 J/g K, which is needed later to calculate uncertainty of enthalpy. This value was subsequently normalized ($\left(\frac{U_R}{R}\right) \times 100$) using the mean nominal value of 2 J/g K. The uncertainty associated with the measuring instrument used to calculate heat capacity was found to be 1.4%. The normalized enthalpy uncertainty was then deducted using the calculated U_{c_p}, values in Table 7 and Eq. (17), and the mean nominal value of 60 J/g, and found to be 1.73%.

5. Conclusions

The main conclusions of the study are listed below:

- DSC results showed that the conversion of CO into CoFA resulted in significant improvements in thermal capability and latent heat of fusion, in addition to a more congruent phase transition temperatures.
- Comparison of OA and LA, DSC results revealed that OA has a higher latent heat of fusion than LA. However, when mixed with CoFA, the mixtures LA/CoFA have a better performance in terms of congruency, phase transition temperatures and latent heat of fusion than OA/CoFA mixtures.
- Thermal conductivity measurement with transient hot wire method showed that the thermal conductivities of the studied combinations were 0.2 and 0.35 W/m K, in liquid and solid states, respectively.
- T-history method was used to measure enthalpy, phase transition temperatures and heat capacity of the mixtures, and the results were compared with those obtained using DSC. Both DSC and T-history results confirmed that the mixture LA/CoFA with the composition $x_{LA} = 0.20$ has the highest heat capacity and enthalpy.
- The thermal performance stability of the studied mixtures after accelerated thermal cycling showed that the mixtures were thermally stable and less than 1% change in phase transition temperature and enthalpy were noticed after 700 cycles. Furthermore, FTIR analysis showed that the mixtures were chemically stable after thermal cycling. Therefore, these new fatty acid mixtures could be a potential BPCM for energy storage in building applications.

Author statement

All persons who meet authorship criteria are listed as authors, and all authors certify that they have participated sufficiently in the work to take public responsibility for the content, including participation in the concept, design, analysis, writing, or revision of the manuscript. Furthermore, each author certifies that this material or similar material has not been and will not be submitted to or published in any other journal before its appearance in the journal of energy storage.

Declaration of Competing Interest

We confirm that there is a financial support for this work by FORMAS, project number 2017-00686. We confirm that the manuscript has been read and approved by all named authors and that there are no other persons who satisfied the criteria for authorship but are not listed. All the authors have approved the order of authors listed in the manuscript. We further confirm that we have given due consideration to the protection of intellectual property associated with this work and that there are no impediments to publication, including the timing of publication,

with respect to intellectual property. In so doing we confirm that we have followed the regulations of our institutions concerning intellectual property. We understand that the Corresponding Author (Assoc. Prof. M. Jebrane) is the sole contact for the Editorial process. He is responsible for communicating with the other authors about progress, submissions of revisions and final approval of proofs of the paper.

Acknowledgments

The authors would like to thank Moritz Sanne from University for Sustainable Development Eberswalde for his support with DSC screening tests. We also acknowledge Ida Lager (Department of Plant Breeding, Swedish University of Agricultural Sciences, Alnarp, Sweden) for her support with GC-MS analyses. The authors also acknowledge the financial support by FORMAS, project number 2017-00686.

References

[1] A. Pasupathy, R. Velraj, R.V. Seeniraj, Phase change material-based building architecture for thermal management in residential and commercial establishments, Renewable Sustainable Energy Rev. 12 (2008) 39–64.
[2] V.V. Tyagi, S.C. Kaushik, S.K. Tyagi, T. Akiyama, Development of phase change materials based microencapsulated technology for buildings: A review, Renewable Sustainable Energy Rev. 15 (2011) 1373–1391.
[3] A. Bland, M. Khzouz, T. Statheros, E.I. Gkanas, PCMs for residential building applications: a short review focused on disadvantages and proposals for future development, Buildings 7 (2017) 78, https://doi.org/10.3390/buildings7030078.
[4] F. Souayfane, F. Fardoun, P.H. Biwole, Phase change materials (PCM) for cooling applications in buildings: a review, Energy Build. 129 (2016) 396–431.
[5] S.E. Kalnæs, B.P. Jelle, Phase change materials and products for building applications: a state-of-the-art review and future research opportunities, Energy Build. 94 (2015) 150–176.
[6] M. Nazari, M. Jebrane, N. Terziev, Bio-based phase change materials incorporated in lignocellulose matrix for energy storage in buildings—a review, Energies 13 (2020) 3065, https://doi.org/10.3390/en13123065.
[7] R.K. Sharma, P. Ganesan, V.V. Tyagi, H.S.C. Metselaar, S.C. Sandaran, Developments in organic solid–liquid phase change materials and their applications in thermal energy storage, Energy Convers. Manage. 95 (2015) 193–228.
[8] M. Kenisarin, K. Mahkamov, Passive thermal control in residential buildings using phase change materials, Renewable Sustainable Energy Rev. 55 (2016) 371–398.
[9] Y. Zhao, X. Min, Z. Huang, Y. Liu, X. Wu, M. Fang, Honeycomb-like structured biological porous carbon encapsulatingPEG: a shape-stable phase change material with enhanced thermal conductivity for thermal energy storage, Energy Build. 158 (2018) 1049–1062.
[10] X. Min, M. Fang, Z. Huang, Y. Liu, Y. Huang, R. Wen, T. Qian, X. Wu, Enhanced thermal properties of novel shape-stabilized PEG composite phase change materials with radial mesoporous silica sphere for thermal energy storage, Sci. Rep. 5 (1) (2015) 1–11.
[11] H. Nazir, M. Batool, F.J.B. Osorio, M.I. Ruiz, X. Xu, K. Vignarooban, P. Phelan, A.M. Kannan Inamuddin, Recent developments in phase change materials for energy storage applications: a review, Int. J. Heat Mass Transfer 129 (2019) 491–523.
[12] F. Kuznik, D. David, K. Johannes, J.J. Roux, A review on phase change materials integrated in building walls, Renewable Sustainable Energy Rev. 15 (2011) 379–391.
[13] Y. Yuan, N. Zhang, W. Tao, X. Cao, Y. He, Fatty acids as phase change materials: a review, Renewable Sustainable Energy Rev. 29 (2014) 482–498.
[14] D. Rozanna, T.G. Chuah, A. Salmiah, T.S.Y. Choong, M. Saari, Fatty acids as phase change materials (pcms) for thermal energy storage: a review, Int. J. Green Energy 1 (4) (2005) 495–513.
[15] N. Sarier, E. Onder, Organic phase change materials and their textile applications: an overview, Thermochim. Acta 540 (2012) 7–60.
[16] R. Baetens, B.P. Jelle, A. Gustavsen, Phase change materials for building applications: a state-of-the-art review, Energy Build. 42 (2010) 1361–1368.
[17] A. Sharma, V.V. Tyagi, C.R. Chen, D. Buddhi, Review on thermal energy storage with phase change materials and applications, Renewable Sustainable Energy Rev. 13 (2009) 318–345.
[18] D. Mathis, P. Blanchet, V. Landry, P. Lagiere, Thermal characterization of bio-based phase changing materials in decorative wood-based panels for thermal energy storage, Green Energy Environ. 4 (2019) 56–65.
[19] D. Mathis, P. Blanchet, V. Landry, P. Lagiere, Impregnation ofWood with Microencapsulated Bio-Based Phase Change Materials for High Thermal Mass Engineered Wood Flooring, Appl. Sci. 8 (12) (2018) 2696, https://doi.org/10.3390/app8122696.
[20] L. Ma, Q. Wang, L. Li, Delignified wood/capric acid-palmitic acid mixture stable-form phase change material for thermal storage, Sol. Energy Mater. Sol. Cells 194 (2019) 215–221.
[21] L. Shilei, Z. Neng, F. Guohui, Eutectic mixtures of capric acid and lauric acid applied in building wallboards for heat energy storage, Energy Build. 38 (2006) 708–711.
[22] M.N.R. Dimaano, T. Watanabe, The capric–lauric acid and pentadecane combination as phase change material for cooling applications, Appl. Therm. Eng. 22 (2002) 365–377.
[23] A. Karaipekli, A. Sari, Preparation, thermal properties and thermal reliability of eutectic mixtures of fatty acids/expanded vermiculite as novel form-stable composites for energy storage, J. Ind. Eng. Chem. 16 (2010) 767–773.
[24] A. Sharma, A. Shukla, C.R. Chen, S. Dwivedi, Development of phase change materials for building applications, Energy Build. 64 (2013) 403–407.
[25] H. Ke, D. Li, H. Zhang, X. Wang, Y. Cai, F. Huang, Q. Wei, Electrospun form-stable phase change composite nanofibers consisting of capric acid-based binary fatty acid eutectics and polyethylene terephthalate, Fibers Polym. 14 (1) (2013) 89–99.
[26] K. Kant, A. Shukla, A. Sharma, Ternary mixture of fatty acids as phase change materials for thermal energy storage applications, Energy Reports 2 (2016) 274–279.
[27] T. Inoue, Y. Hisatsugu, R. Ishikawa, M. Suzuki, Solid–liquid phase behavior of binary fatty acid mixtures: 2. Mixtures of oleic acid with lauric acid, myristic acid, and palmitic acid, Chem. Phys. Lipids 127 (2) (2004) 161–173.
[28] T. Inoue, Y. Hisatsugu, R. Yamamoto, M. Suzuki, Solid–liquid phase behavior of binary fatty acid mixtures: 1. oleic acid/stearic acid and oleic acid/behenic acid mixtures, Chem. Phys. Lipids 127 (2) (2004) 143–152.
[29] G. Lawer-Yolar, B. Dawson-Andoh, E. Atta-Obeng, Novel phase change materials for thermal energy storage: evaluation of tropical tree fruit oils, Biotechnol. Rep. 24 (2019) e00359.
[30] R. Thaib, M. Amin, H. Umar, Thermal properties of beef tallow/coconut oil bio PCM using T-history method for wall building applications, Eur. J. Eng. Res. Sci. 4 (11) (2019) 38–40.
[31] C. Ahamed Saleel, M. Abdul Mujeebu, Salem Algarni, Coconut oil as phase change material to maintain thermal comfort in passenger vehicles, J. Therm. Anal. Calorim. 136 (2019) 629–636.
[32] M. Irsyad, Heat transfer characteristics of coconut oil as phase change material to room cooling application, in: IOP Conference Series: Earth and Environmental Science 60, IOP Publishing, 2017, 012027.
[33] S. Kahwaji, M.A. White, Edible oils as practical phase change materials for thermal energy storage, Appl. Sci. 9 (8) (2019) 1627.
[34] P. Gallart-Sirvent, M. Martín, G. Villorbina, M. Balcells, A. Solé, C. Barrenche, L. F. Cabeza, R. Canela-Garayoa, Fatty acid eutectic mixtures and derivatives from non-edible animal fat as phase change materials, RSC Adv. 7 (39) (2017) 24133–24139.
[35] D. Zhao, X. Qian, X. Gu, S.A. Jajja, R. Yang, Measurement techniques for thermal conductivity and interfacial thermal conductance of bulk and thin film materials, J. Electron. Packag. 138 (4) (2016), 040802.
[36] F. Frusteri, V. Leonardi, S. Vasta, G. Restuccia, Thermal conductivity measurement of a PCM based storage system containing carbon fibers, Appl. Therm. Eng. 25 (2005) 1623–1633.
[37] A. Sarı, A. Karaipekli, Thermal conductivity and latent heat thermal energy storage characteristics of paraffin/expanded graphite composite as phase change material, Appl. Therm. Eng. 27 (2007) 1271–1277.
[38] A. Franco, An apparatus for the routine measurement of thermal conductivity of materials for building application based on a transient hot-wire method, Appl. Therm. Eng. 27 (2007) 2495–2504.
[39] J.N.W. Chiu, V. Martin, Submerged finned heat exchanger latent heat storage design and its experimental verification, Appl. Energy 93 (2012) 507–516.
[40] H. Badenhorst, L.F. Cabeza, Critical analysis of the T-history method: a fundamental approach, Thermochim. Acta 650 (2017) 95–105.
[41] P. Tan, M. Brütting, S. Vidi, H.P. Ebert, P. Johansson, A.S. Kalagasidis, Characterizing phase change materials using the T-History method: on the factors influencing the accuracy and precision of the enthalpy-temperature curve, Thermochim. Acta 666 (2018) 212–228.
[42] S.N. Gunasekara, R. Pan, J.N.W. Chiu, V. Martin, Polyols as phase change materials for surplus thermal energy storage, Appl. Energy 162 (2016) 1439–1452.
[43] S.N. Gunasekara, J.N.W. Chiu, V. Martin, P. Hedström, The experimental phase diagram study of the binary polyols system erythritol-xylitol, Sol. Energy Mater. Sol. Cells 174 (2018) 248–262.
[44] A. Solé, L. Miró, C. Barreneche, I. Martorell, L.F. Cabeza, Review of the T-history method to determine thermophysical properties of phase change materials (PCM), Renewable Sustainable Energy Rev. 26 (2013) 425–436.
[45] P. Zhao, Q. Yue, H. He, B. Gao, Y. Wang, Q. Li, Study on phase diagram of fatty acids mixtures to determine eutectic temperatures and the corresponding mixing proportions, Appl. Energy 115 (2014) 483–490.
[46] G. Çaylı, S. Küsefoğlu, A simple one-step synthesis and polymerization of plant oil triglyceride iodo isocyanates, Appl. Polymer 116 (4) (2010) 2433–2440.
[47] T. Senphan, S. Benjakul, Chemical compositions and properties of virgin coconut oil extracted using protease from hepatopancreas of Pacific white shrimp, Eur. J. Lipid Sci. Technol. 118 (2016) 761–769.
[48] C.P. Tan, Y.B. Che Man, Differential scanning calorimetric analysis of palm oil, palm oil based products and coconut oil: effects of scanning rate variation, Food Chem. 76 (1) (2002) 89–102.
[49] T.S.T. Mansor, Y.B. Che Man, M. Shuhaimi, Employment of Differential Scanning Calorimetry in Detecting Lard Adulteration in Virgin Coconut Oil, J. Am. Oil Chem. Soc. 89 (2012) 485–496.
[50] S. Ueno, A. Miyazaki, J. Yano, Y. Furukawa, M. Suzuki, K. Sato, Polymorphism of linoleic acid (*cis*-9, *cis*-12-Octadecadienoic acid) and a-linolenic acid (*cis*-9, *cis*-12, *cis*-15-Octadecatrienoic acid), Chem. Phys. Lipids 107 (2000) 169–178.
[51] V. Wylen, G. John, R.E. Sonntag, C. Borgnakke, Fundamentals of classical thermodynamics, Wiley, New York, 1976.

[52] R.K. Sharma, P. Ganesan, V.V. Tyagi, Long-term thermal and chemical reliability study of different organic phase change materials for thermal energy storage applications, J. Therm. Anal. Calorim. 124 (3) (2016) 1357–1366.
[53] A. Sari, Thermal energy storage properties of mannitol–fatty acid esters as novel organic solid–liquid phase change materials, Energy Convers. Manage. 64 (2012) 68–78.
[54] S. Xu, L. Zou, X. Ling, Y. Wei, S. Zhang, Preparation and thermal reliability of methyl palmitate/methyl stearate mixture as a novel composite phase change material, Energy Build. 68 (2014) 372–375.
[55] S. Liu, L. Han, S. Xie, Y. Jia, J. Sun, Y. Jing, Q. Zhang, A novel medium-temperature form-stable phase change material based on dicarboxylic acid eutectic mixture/expanded graphite composites, Sol. Energy 143 (2017) 22–30.
[56] N. Sheng, T. Nomura, C. Zhu, H. Habazaki, T. Akiyama, Cotton-derived carbon sponge as support for form-stabilized composite phase change materials with enhanced thermal conductivity, Sol. Energy Mater. Sol. Cells 192 (2019) 8–15.
[57] Z. Yang, Y. Deng, J. Li, Preparation of porous carbonized woods impregnated with lauric acid as shape-stable composite phase change materials, Appl. Therm. Eng. 150 (2019) 967–976.
[58] H. Fauzi, H.S.C. Metselaar, T.M.I. Mahlia, M. Silakhori, Thermo-physical stability of fatty acid eutectic mixtures subjected to accelerated aging for thermal energy storage (TES) application, Appl. Therm. Eng. 66 (2014) 328–334.
[59] N. Zhang, Y. Yuan, Y. Du, X. Cao, Y. Yuan, Preparation and properties of palmitic-stearic acid eutectic mixture/expanded graphite composite as phase change material for energy storage, Energy 78 (2014) 950–956.
[60] A. Sari, Eutectic mixtures of some fatty acids for latent heat storage: thermal properties and thermal reliability with respect to thermal cycling, Energy Convers. Manage. 47 (2006) 1207–1221.
[61] T. Matsui, M. Yoshida, H. Yamasaki, Y. Hatate, Thermal properties of multicomponent fatty acids as solid–liquid phase change materials for cooling applications, Chem. Eng. Commun. 194 (1) (2007) 129–139.
[62] A. Karaipekli, A. Sari, K. Kaygusuz, Thermal Properties and Long-term Reliability of Capric Acid/Lauric Acid and Capric Acid/Myristic Acid Mixtures for Thermal Energy Storage, Energy Sources, Part A 30 (13) (2008) 1248–1258.
[63] H. Fauzi, H.S.C. Metselaar, T.M.I. Mahlia, M. Silakhori, H. Chyuan Ong, Thermal characteristic reliability of fatty acid binary mixtures as phasechange materials (PCMs) for thermal energy storage applications, Appl. Therm. Eng. 80 (2015) 127–131.
[64] S. Himran, A. Suwono, G.A. Mansoori, Characterization of Alkanes and Paraffin Waxes for Application as Phase Change Energy Storage Medium, Energy Sources 16 (1) (1994) 117–128.
[65] S.J. Kline, F. McClintock, Describing uncertainties in single-sample experiment, Mech. Eng. 75 (1953) 3–8.
[66] R.J. Moffat, Describing the uncertainties in experimental results, Exp. Therm. Fluid Sci. 1 (1) (1988) 3–17.
[67] H.W. Coleman, W.G. Steele, Experimentation, Validation, and Uncertainty Analysis for Engineers, 3rd ed., John Wiley and Sons Inc., Hoboken, New Jersey, 2009.